Přírodovědecká fakulta
Faculty of Science

Jihočeská univerzita v Českých Budějovicích
University of South Bohemia in České Budějovice

Creating an in-vitro model system for studying phase separation in virus assembly

Bachelor thesis

Katharina Wiener

Supervisor: Roman Tůma, Mgr. Ph.D.

Co-Supervisor: Barbora Kaščáková, Mgr.

České Budějovice 2021

Wiener K., 2021: Creating an in-vitro model system for studying phase separation in virus assembly, Bc. Thesis, in English 58 p. Faculty of Science, University of South Bohemia, České Budějovice, Czech Republic.

Annotation:

This thesis focuses on the study of the μNS protein of the avian reovirus and as this virus is causing considerable annual losses in the poultry industry, understanding its replicative cycle on a molecular basis is highly anticipated. One area of interest is hereby the formation of so-called viroplasms via liquid-liquid phase separation (LLPS) of the μNS protein. The exact processes involved in LLPS, however, remain mostly unknown. By establishing an in-vitro model system we tried to elucidate the environmental conditions needed for phase separation, in order to gain a better understanding of the viral replicative cycle, as well as LLPS in general.

Declaration:

I hereby declare that I have worked on my bachelor's thesis independently and used only the sources listed in the bibliography.

I hereby declare that, in accordance with Article 47b of Act No. 111/1998 in the valid wording, I agree with the publication of my bachelor thesis, in full to be kept in the Faculty of Science archive, in electronic form in publicly accessible part of the STAG database operated by the University of South Bohemia in České Budějovice accessible through its web pages. Further, I agree to the electronic publication of the comments of my supervisor and thesis opponents and the record of the proceedings and results of the thesis defence in accordance with aforementioned Act No. 111/1998. I also agree to the comparison of the text of my thesis with the Theses.cz thesis database operated by the National Registry of University Theses and a plagiarism detection system.

České Budějovice, ...

.....

Katharina Wiener

Acknowledgements

First, I would like to thank my supervisor Roman Tůma, who supported me throughout the whole process of working on and writing my thesis. With his expertise and dedication to the project he helped me understand the importance and relevance of the topic and constantly gave me new input and valuable feedback.

Next, I would like to bring forward my sincerest gratitude for my Co-Supervisor Barbora Kaščáková, who was with me at all stages of the experimental work. I deeply appreciate the time and effort she invested into teaching me the fundamental techniques of molecular biology. I also want to thank her for her seemingly endless enthusiasm, which helped me to continue work in times when experiments did not go as planned and needed to be repeated several times.

Also, I thank Tomáš Fessl for introducing me to the world of Fluorescence Spectroscopy and kindly letting me conduct experiments on his microscope, and Joel Crossley for helping me with FCS.

Finally, I would like to say thank you to everybody at Makrokomplex for welcoming me to their lab and supporting me whenever needed.

Table of Contents

List of abbreviation

AMP	ampicillin
AE	anion exchange chromatography
APS	Ammonium Persulfate
CD	Circular Dichroism
CBB	Coomassie 250 Brilliant Blue
DMSO	Dimethyl Sulfoxide
ddH_2O	double distilled water
FCS	Fluorescence Correlation Spectroscopy
HisTrap	histidine-tagged protein purification columns
HRP	Horseradish peroxidase
IPTG	isopropyl b-D-1- thiogalactopyranoside
kb	kilobase
kDA	kilodalton
LB	lysogeny broth
mRNA	messenger RNA
OD_{600}	optical density measurement at 600 nm
PBS	phosphate-buffered saline
PAGE	polyacrylamide gel electrophoresis
PEG	polyethylene glycol
PCR	polymerase chain reaction
PVDF	polyvinylidene fluoride
SEC	size exclusion chromatography
SDS	sodium dodecyl sulfate
TEMED	tetramethylethylenediamine
UV	ultraviolet

1. Introduction

1.1 The Avian reovirus

Being part of the Orthoreovirus genus, the Avian reovirus (ARV) belongs to the family of *Reoviridae* (Attoui et al., 2000; Mertens, 2004). Members are characterized by non-enveloped, icosahedral structure surrounded by a double capsid and their dsRNA genome, which is separated into ten to twelve segments coding for ten to fourteen gene products, depending on the type of virus. Replication takes place in the cytoplasm of the host cell within membrane-less inclusions that are often called "viral factories" or "viroplasms" and will be explained in detail later. Vertebrates, invertebrates, plant and fungi can function as a host and examples can be found globally (ViralZone.org). Besides ARV, four other species are classified in the genus. These can again be separated into two groups. Those, which cause cell-cell fusion, termed fusogenic and those not triggering such an event, i.e. non-fusogenic. While the avian reovirus shows a fusogenic phenotype, as do two other members, opposed to the non-fusogenic mammalian reovirus. Other fusogenic reoviruses can only be found in reptiles. (Mertens, 2004). The two main groups are the mammalian (MRV) and avian reoviruses (ARV), which differ in their fusogenicity (only ARV causes fusion) and hemagglutination activity (only MRV) (Nibert and Schiff, 2001).

As the name suggests, the avian reovirus infects poultry fowls and causes a range of diseases related to the respiratory organs, myocarditis, an inflammation of the heart muscle, hepatitis and arthritis. Mostly younger birds are susceptible to the infection and the virus is thought to be transmitted orally but it is further suggested that transmission through respiration or via eggs could be possible (Benavente & Martínez-Costas, 2007).

1.1.1 Virion Structure

The nonenveloped icosahedral virions have an external diameter of 85 nm and a buoyant density of 1.37 g/mL (Spandidos & Graham, 1976; Zhang et al., 2005). This structure (Figure 1) is built up from two concentric protein shells, forming the inner and outer capsid and made by the 8 structural proteins (λ A, λ B, λ C, μA, μB, σC, σA, σB) encoded in the genome. All of the mentioned proteins are the final products of translation, except μB, which is post-translationally cleaved into two parts at either the N- or C-terminus, called μBN or μBC, respectively. The inner capsid is formed by the protein λ A and shows to be a shell, which is stabilized and connected to the outer capsid by 150 nodules of the σA protein. σA further

prevents any penetration of foreign proteins and RNA into the core. Also attached to the inner shell, and pointing outwards are 12 five-fold turrets formed by pentamers of λ C. These form channels, where the 5’ capping of the viral mRNA is presumably performed (Martinez-Costas et al., 1995). Further, the outer part of the turret works as a site for binding of the σC protein, which is responsible for attachment to the host cell. As mentioned earlier, the nodules of the σA protein function as contacts to the outer capsid and do so by trimers of μBC, which then allow μB to form the outer shell with the help of σB (Benavente & Martínez-Costas, 2007). In vitro experiments using low ionic strength buffers or by treatment with NaCl combined with low concentrations of trypsin or chymotrypsin showed, that by removing the outer capsid proteins σB, μB, μBC and μBN, the virion core remained infectious and transcriptionally active until also the σC protein was removed by buffers with a high concentration of protease (Martínez- Costas et al., 1997).

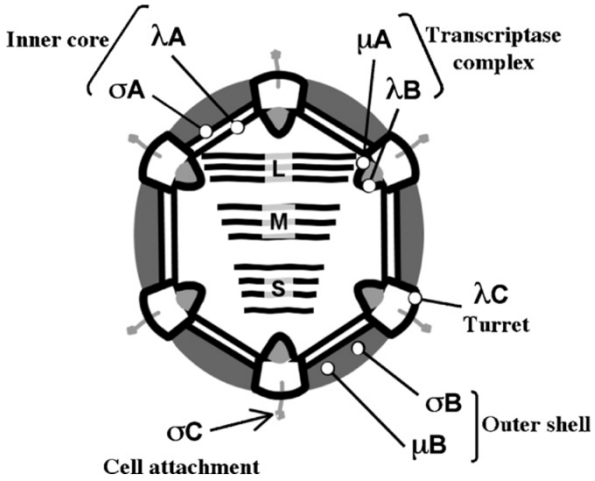

Figure 1 **Schematic representation of the Avian Reovirus particle** (Benavente & Martínez-Costas, 2007)

1.1.2 Genome

In the core inside the previously described capsid, the virus contains 10 double stranded RNA segments belonging to three classes (L (large), M (medium), S (small)) based on their length. The classes L and M each contain three segments, whereas, in the S-class, four can be found. All segments are consecutively numbered and categorized (L1-L3, M1-M3, S1-S4) (Spandidos & Graham, 1976). Each of these segments, except for S1 which encodes 3 products, is responsible for the coding of one primary translation product. It was found that all positive mRNA strands include a 5´cap and exhibit the same 7 nucleotides (GCUUUUU) at the 5´end and the same 5 nucleotides (UCAUC) at the 3´end. These conserved sequences could probably

act as regulatory and binding sequences for transcription, replication and/or encapsidation of the transcripts (Benavente & Martínez-Costas, 2007).

As there are nine monocistronic segments and one that codes for three, 12 primary translational products can be expressed. Eight of those are considered structural, as they are part of the mature virion, and four nonstructural, which are highly expressed in the infected cell during the replicative cycle but do not get incorporated into the virion. Just as the genomic segments itself, the expressed proteins are labelled alphabetically according to their electrophoretic mobility (described in Table 1). Table 1 further lists the confirmed and putative functions of each protein and states the genome segment each belongs to , as well as the distribution throughout the virion.

Table 1 **List of all genome segments, the proteins found in each segment and their respective functions** (Benavente and Martínez-Costas, 2007).

Genome segment	Protein	Distribution	Function
L1	λA	Inner core	Core shell scaffold
L2	λB	Inner core	Putative transcriptase
L3	λC	Turrets	Capping enzyme
M1	μA	Inner core	Putative transcriptase co-factor
M2	μB, μBN, μBC	Outer capsid	Penetration
M3	μNS, μNSC, μNSN	Nonstructural	Formation of viral factories and protein recruitment
S1	σC	Outer capsid	Cell attachment
	p10	Nonstructural	Permeabilising/fusogenic
	p17	Nonstructural	Unknown
S2	σA	Inner core	dsRNA binding, anti-interferon activity
S3	σB	Outer capsid	Unknown
S4	σNS	Nonstructural	ssRNA binding

1.1.3 Replicative Cycle

For a virus to start replication, it first has to enter the host cell. In the case of the non-enveloped avian reovirus, this is done by receptor-mediated endocytosis, in which the outer capsid protein σC interacts with the cell surface receptors (Figure 2). How these receptors work precisely is yet to be identified. In the case of mammalian reovirus, the junction adhesion molecule (JAM) was identified to be the receptor for virus attachment, by interacting with the σ1 protein of the virus. JAM belongs to the superfamily of immunoglobin, and it was shown, that it regulates virus attachment, infection and intracellular signalling (Barton et al., 2001). After crossing the membrane, the parent virion has to undergo proteolytic processing, known as uncoating and performed within endosomes. Previous studies have pointed out the importance of acidification of the endosomes because when adding neutralizing agents such as ammonium chloride directly after the infection, the uncoating and further the replication was inhibited (Duncan, 1996; Labrada et al., 2002). By cleaving the outer capsid proteins, the viral cores can be released into the cytoplasm of the host cell and transcription can start.

The mRNA of the avian reovirus has two functions: first, they are genomic precursors for the minus strand of the next generation, and second, they are used for viral protein synthesis. To synthesize the 10 viral mRNAs, out of which 9 are monocistronic, the negative strands are used as template and the process is catalysed by several copies of the dsRNA-dependent RNA polymerase associated with the virion (Benavente & Martínez-Costas, 2007). Experimental evidence by Martinez-Costas et al., 1995, show that these polymerases perform mRNA synthesis inside the core. This is supported by previous studies of the mammalian reovirus, which state that the λ3 protein (encoded on the L1 segment) possesses certain segments, which are conserved in all viral RNA polymerases (Morozov, 1989). Further, early kinetic studies and hybridization experiments (Banerjee & Shatkin, 1970), suggested a simultaneous transcription of all genome segments, leading to the assumption that several polymerases are involved in the process. Lacking a polyadenylated 3´tail and possessing a type-1 cap at their 5´end, the transcribed mRNA contains on each end additional untranslated regions (Martínez-Costas et al., 1995). The cap structure at the 5´end is thought to be gained while the transcribed mRNA is leaving the inner core through channels created by pentamers of the λC protein (Zhang et al., 2005). Figure 2 shows a schematic representation of the replicative cycle and it can be seen, that opposed to transcription, taking place inside the core, the then mature mRNA is translated in the cytoplasm of the host cell.

While after transcription, the mRNAs are present at approximately the same amount, the abundancy of expressed proteins strongly varies post-translationally, leading to the assumption that gene expression is regulated mainly during translation. Regulation is most likely caused by the different structural aspects of viral mRNAs, but not yet proven.

Before the virus can assemble again, an environment suitable for this purpose has to be formed. This is principally done by the non-structural protein µNS, which forms viral inclusion or often referred to as viral factories. (A more detailed explanation can be found in section 1.2) Based on preliminary results it is hypothesized, that these are generated by a liquid-liquid phase separation to give rise to a region with a denser distribution of proteins. Phase-dense regions were already identified in the mammalian reovirus and believed to function as viral factories (Broering et al., 2002). Inside these formations, which are not enclosed by any membrane or associated with other organelles, viral morphogenesis is thought to take place. Metabolic pulse-chase radiolabelling with cell fractionation combined with antibody immunoprecipitation have shown, that with the first 30 min after translation, the structural proteins are assembled to form the viral core (Touris-Otero et al., 2004). Addition of the capsid proteins then completes the assembly of new virions. How the mature virus then exits these inclusions, is so far unknown and can only be speculated. Options include that the viral particle simply exits the phase-dense region or that the inclusion body undergoes dissolution caused by some conditional change of the environment.

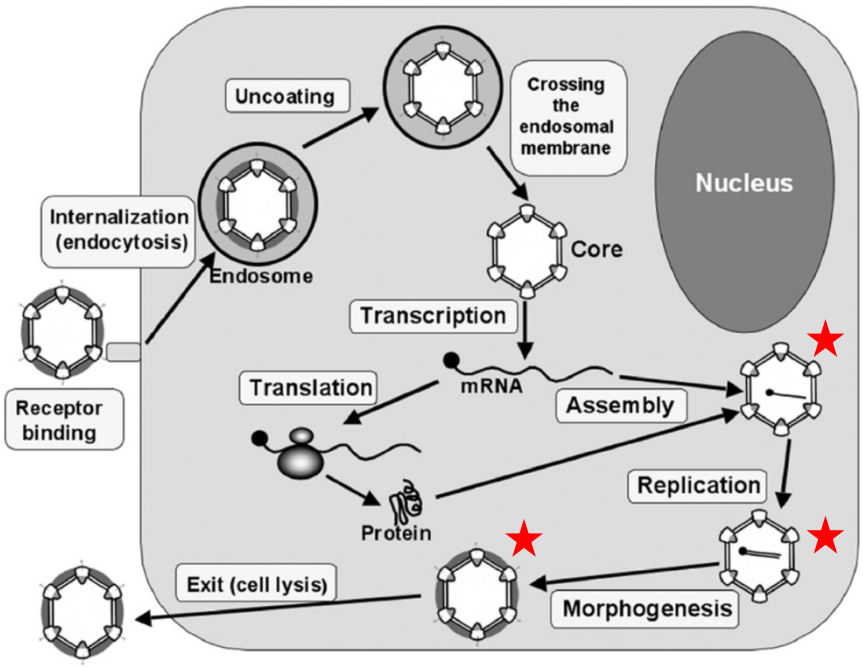

Figure 2 **Schematic representation of the replicative cycle of the Avian Reovirus** (Benavente & Martínez-Costas, 2007)
Steps marked with a ★ take place within membrane-less inclusions

1.2 The µNS protein

µNS is a nonstructural protein encoded by the M3 gene in the avian reovirus which has a molecular weight of 70 kDa. Other non-structural proteins are σNS (on the S4 segment), p10 and P17 (both on the S1 segment), which together with µNS were only found in cells, which were infected and not in viral particles itself and were hence given the designation of not being structural components (Brandariz-Nuñez et al.; 2010). Despite not being directly involved in the structure of the virus, the play an important role as they are used as viral factories within the infected cells, in which virus replication takes place. That these membrane-less organelles are formed by µNS was deduced after expressing it in absence of any other viral components and formation could still be observed. Following this, co-expression of µNS, λA and σNS was performed and it was found, that µNS, after forming inclusion bodies by itself, recruits λA, σNS and possibly other viral proteins, which then allow binding of virus mRNA (Tourís-Otero et al.; 2004).

Investigating in which parts of the sequence are necessary for successful inclusion body formation, it was found, that the minimal region needed lies between residues 448 and 635. (Figure 3) Within this sequence two coiled-coils were predicted, whereby the first, C1, can be found comprising residues right at the beginning of the needed sequence, namely 448 to 477 and the second, C2, from 539 to 605. It also includes the two amino acids His570 and Cys572, which were found to be present in every µNS derivative of other virus species and are a crucial factor fur successful inclusion body formation. C1 is said to be able of self-association and the provider of needed interaction domains. In between a spacer, termed IC, was found covering 61 residues connecting the two coiled domains. Finally, at the end of the essential sequence, we find the so-called C-tail from residue 605 to 635. Further deletions demonstrated that C-terminal 187 residues are sufficient to cause inclusion formation while the very C-terminal 30-residues play a crucial role in the establishment of the main monomer-monomer contacts, which control the efficiency of inclusion formation (Brandariz-Nuñez et al.; 2010).

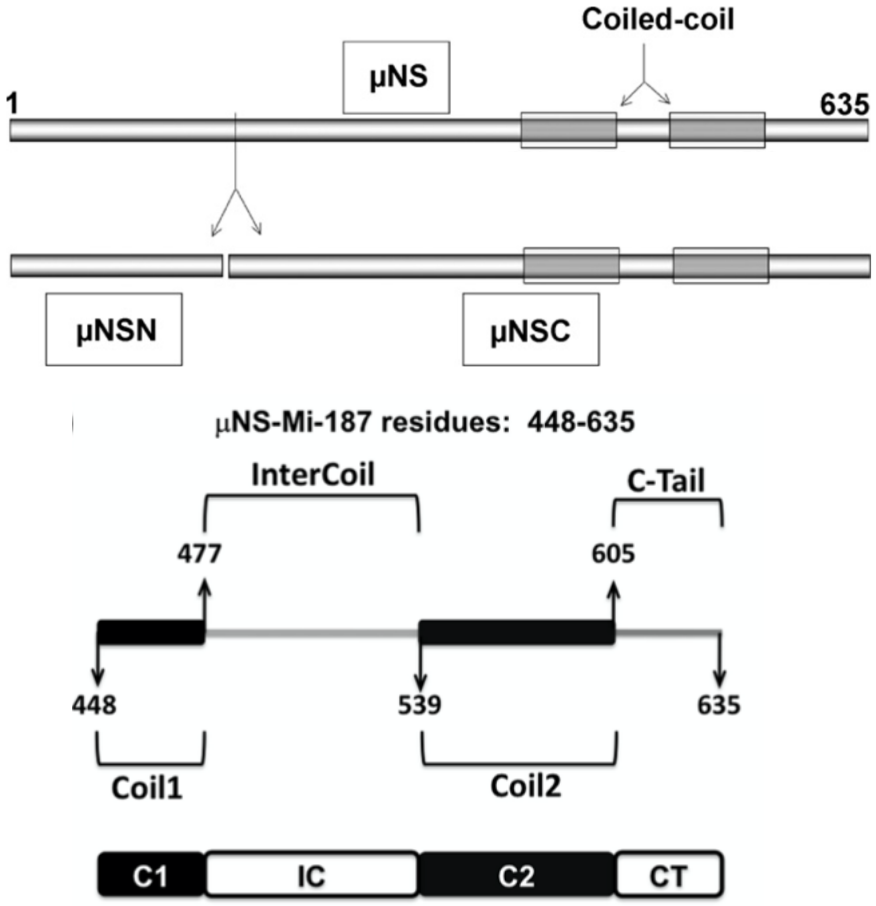

Figure 3 Upper panel: **schematic representation of the full length μNS**: predicted coiled-coils near the C-terminus; Below, a yet unknown site cleaving μNS into μNSN and μNSC in infected cells is shown (Benavente & Martínez-Costas, 2007).

Lower panel: **Schematic drawing of the minimal region needed for viroplasm formation of μNS**: The two coils at 448-477 and 539-605 were experimentally determined and are enclosing the so-called Inter Coil region (Brandariz-Nuñez et al.; 2010).

What has also been stated by the research of Brandariz-Nuñez et al. is the fact, that inclusions formed are neither connected nor dependent on the vast microtubular system within the cytoplasm. This contrasts findings from studies concerning the mammalian reovirus, in which the viroplasm-forming protein μNS associates with μ2, which then relocates it to microtubules. The combination of these two results in globular-shaped inclusions similarly to when μNS is expressed individually. By treatment with nocodazole it was shown that only an intact microtubular system allows the formation of μNS / μ2 inclusions. (Broering et al.; 2002) However, in the case of the avian reovirus, even in cells with induced destruction of this network, inclusion bodies were still formed and showed no difference to cells with fully functioning microtubules. The globular bodies can therefore freely move and show highly dynamic properties such as in other studied phase separations. (Brandariz-Nuñez et al.; 2010)

The mentioned dynamic properties were also already observed by fluorescence microscopy and events of growth and fusion were detected over time in live cell imaging (B. Kascakova, Z. Franta and R. Tuma, unpublished). Over time a continuous growth could be detected accompanied by a decrease in the number of single bodies. After 72 h the amount was in some cells reduced to one single large inclusion, which surrounded the area of the nucleus (Brandariz-Nuñez et al.; 2010). Such behaviour is suggestive of fluid character of vioplasms and their possible formations by liquid-liquid phase separation (LLPS) (Brangwynne, 2011).

1.3 Phase separation in biological systems

Phase separation is a phenomenon, which occurs when many different components are present in one mixture which becomes thermodynamically unstable. These mixtures can then undergo a separation into their constituents which then form spatially distinct regions with differing compositions mostly caused by external factors such as temperature, salt concentration, protein concentration and composition (Jacobs & Frenkel, 2017). This compartmentalization often occurs in supersaturated solutions in a spontaneous manner and in the form of globular liquid-like droplets, which bear a high-concentration region on the inside, surrounded by a low-concentration environment. However, phase separation can also form gel or solid structures within the cytosol (Brangwynne, 2011). In our case, we are mostly interested in the liquid-liquid separation as we suspect it plays an important role in virus assembly.

To understand the behaviour of these droplets, it has to be mentioned, that also “simple liquids” display a detectable dynamic structure in which molecules exhibit short-range order due to isotropic attractive potentials. Proteins, in contrast, can also be present in either well-mixed or spatially organized droplets (as it is the case with μNS after LLPS), which are created by non-covalent bonds (Boeynaems et al., 2018). Those droplets, or as in a cellular context, membrane-less organelles, show strong similarities to materials known in polymer chemistry and are therefore sometimes referred to as associative polymers. This term arises from the mentioned interactions and physical links within them. Additionally, those bodies have the ability to stably coexist in two distinct (liquid) phases and can easily change material states. The establishment of those phases is created by so-called de-mixing events, in which the randomly mixed particles of the liquid solution start to form clusters and go over into a two-phase state. For this to occur, only slight changes in either component concentrations or composition changes of the surrounding are needed (Jacobs & Frenkel, 2017). Further, it was

argued by Jacobs and Frenkel, that in biological systems, multicomponent mixtures favour the occurrence of such de-mixing events and the distinct phases can be selected by tuning the intermolecular interactions. Multicomponent systems are defined as *mixtures which consist of several pure (individual) substances (components)* (Boyarsky & Semenov, 2011), whereby an increase of numbers of components results in only a single condensation phase transition and not in further de-mixing events of the separated solutions (Jacobs & Frenkel, 2017).

Multivalency of protein interactions showed to be a crucial factor for phase separation to occur. Being able to be linked together in many different ways seems to drive LPPS, while not losing its dynamics which would lead to solidification. So-called IDRs, intrinsically disordered regions, within the protein often display simple, repetitive sequences and serve as linkers and further as multivalent interaction sites for phase transitions to occur. These IDRs have been found in several proteins involved in formation of membrane-less organelles inside the cell and have therefore been drawing attention to them over the last years. Inside the IDRs we can often find a majority of uncharged polar side chains, negatively charged amino acids or aromatic residues, which seem to be arranged in a well-defined and repetitive manner (=SLIM-short linear interaction motifs). In the specific case of μNS an eight amino acid long residue has been identified at the protein's C-terminal, which consist of such amino acid types and therefore suggests the presence of an IDR:

Phe (aromatic) - Ser (polar, uncharged) - Val (nonpolar) - Pro (polar, uncharged) ‑ Thr (polar, uncharged) ‑ Asp (negatively charged) ‑ Glu (negatively charged) - Leu (nonpolar)

Nevertheless, this region is not highly conserved when investigating homologs of the avian orthoreovirus and aquareoviruses, but shows to always terminate with Leucine, includes at least one acidic and no basic residues (Broering et al., 2005). Further, its exact role in inclusion formation is yet to be determined.

Additionally, the μNS sequence was analysed using the DEPICTER software (Barik, A., et al., 2019), which predicted few disordered regions (Figure 4) , including disordered protein (second lane) and DNA binding sites (fourth lane).

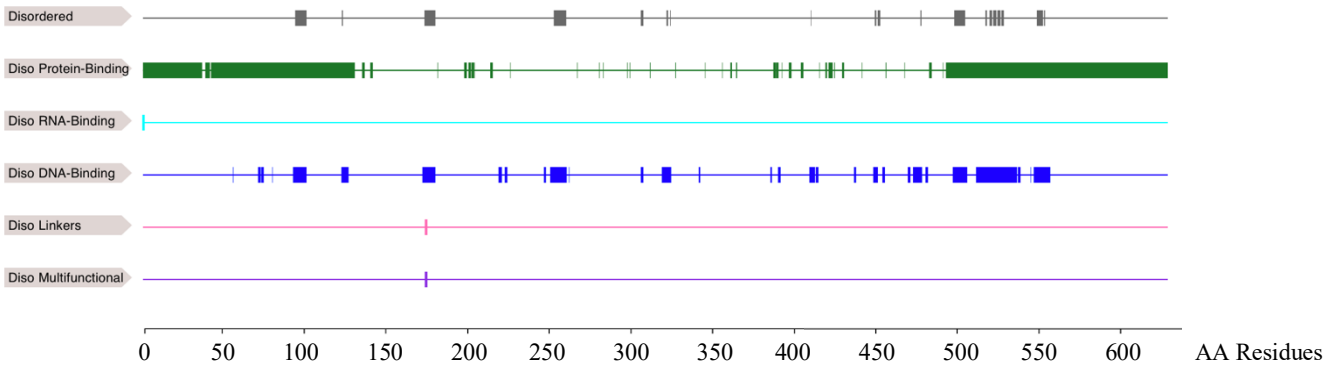

Figure 4 **disordered regions on the µNS sequence** as predicted by DEPICTER (Barik, A., et al.; 2019)

Based on the gained knowledge of IDRs, it was concluded, that phase separation is driven by several different forces, such as hydrogen bonds, electrostatic interaction (charge-charge and dipole-dipole), pi-pi and cation-pi interactions. (Lin et al., 2015).

Another driving factor of liquid-liquid phase separation seems to be the interaction with present RNAs. However, it was shown in experiments performed by Lin et al. that in most proteins, the addition of RNA only has a favourable effect, if IDRs are present as well. They then concluded synergic effect between the two. As the µNS protein does not show any direct binding to RNA it seems irrelevant to consider such interactions. However, the σNS protein, which is recruited into the inclusion by µNS, has shown to bind RNA (Tourís- Otero et al.; 2004) and this could possibly alter the conditions for phase behaviour. Nevertheless, this assumption is still to be experimentally verified or refuted in future.

To investigate driving factors of droplet formation, the team of Lin et al. examined known components of RNP granules, which undergo LLPS. By doing so, following conclusion where made (which hold for the system in question, but could presumably be valid for others too): First, crowding agents such as polyethylene glycol can drive phase separation if no RNA is present and the protein concentration is high enough (Lin et al., 2015). Second, different proteins and therefore different IDRs promote various morphological appearances of the liquid droplets. Third, the addition of RNA also triggers aggregation over time and drives the formation of filamentous structures (Lin et al., 2015). However, as in vivo observations showed, fibre formation is not only caused by phase separation but presumably favoured due to higher protein concentrations in the droplets. Concerning the effect of time, two observation were made: First, their shape mostly changes from a well-defined globule to a more irregular shape. Second, salt-resistance increases (in the specific case of the RNP granule system) as the more time pass, the more difficult it becomes to reverse phase separation caused by low salt

concentrations. At 24 hours the globules tend to be completely resistant towards increasing amounts of salt. The last major finding was a change in mobility over time. This was visualized by Fluorescence Recovery After Photobleaching (FRAP), in which generally the fluorescent tag of a e.g. protein is excited first and then irreversibly inactivated (=bleached) by a high intensity laser beam combined with the presence of molecular oxygen. Following, the time is measured until unbleached molecules from the surroundings replace the bleached ones by diffusion. By measuring this so-called recovery time and plotting it against the relative fluorescence intensity, one can establish a ratio between the immobile and mobile fractions, where the immobile includes all molecules participating in the exchange. An increase in the recovery time can therefore conclude a "slowing down" of molecules. As shown in experiments performed by Lin et al., 2015 concerning the droplet behaviour of RNP granules, the fluorescence recovery time increases up until the point they become completely static (schematic representation Figure 5; hypothetical data). Their findings show, that in the first hour after initiation the fluorescently labelled region of the droplet would recover with half-lives between 19 and 64 seconds. Further, the fractional recovery lies between 0.3 to 0.9, meaning that most of the fluorescence could be detected again after recovery. Within 14 to 24 hours, these recovery values constantly decreased, while the half-lives increased over time. At the end of the measurements, the fluorescent regions no longer recovered, suggesting a static state after a certain time. This behaviour correlates with the time in which the droplets change their morphologies. Those remaining longer as liquid globules also showed to be more dynamic compared to such that rather quickly changed shape (Lin et al., 2015).

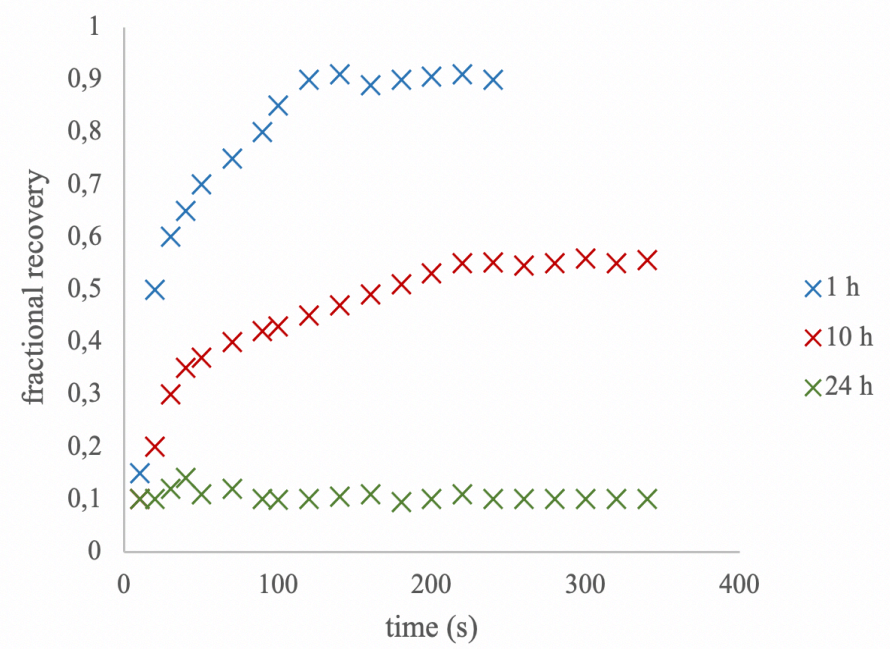

Figure 5 **Hypothetical data** illustrating the concept of fractional recovery after photobleaching. Differently colored data points show hypothetical results after 1, 10 or 24 hours.

Not only can the phase-separated droplets move and change shape, but they are further able to recruit other proteins into them to form bigger structures. This is most likely driven by the presence of IDRs. If in both proteins such regions are present, they tend to bind and assemble into a single droplet. This process is catalysed by the concentration of IDRs, the higher the more likely phase separation occurs (Lin et al., 2015).

Within the cell, membrane-less organelles are still to be studied more thoroughly, but several important functions have already been explored. Table 2 summarizes some of the best-known examples, their localization and related purpose.

Table 2 **Examples of membraneless organelles with their main function and localization in the cell** (Brangwynne, 2011)

Name	Other names/related structures	Localization	Function
Nucleolus	—	Nucleus	Ribosome subunit assembly
Cajal bodies	CBs, spheres, coiled bodies	Nucleus	RNA splicing, processing
Centrosomes	—	Mitotic spindle poles	Microtubule nucleation/ organization
Processing bodies	P bodies, GW bodies	Cytoplasm	RNA degradation, processing
Paraspeckles	—	Nucleus	Processing, nuclear retention of RNA
P granules	Germ granules, nuage, germ plasm	Cytoplasm, nuclear pore-associated	Germ cell specification
Speckles	B-Snurposomes, interchromatin granule clusters	Nucleus, often CB-associated	RNA splicing, processing

Additionally, phase separation can be driven by other factors, such as virus infection, which is studied in this thesis. In the case of the orthoreovirus, the droplets play a crucial role in virus morphogenesis and assembly of the new virion. The reason for these steps to take place within liquid-like droplets is the dynamics and structure of such. With not having a surrounding membrane, the viral mRNAs can easily be recruited into the dense phase by interaction with binding domains of the concentrated viral proteins. Inside, the molecules necessary for virus assembly are brought together more closely, while not restricting their mobility. This then leads to a higher rate of molecular interactions thus catalysing virus assembly (Brangwynne, 2011).

1.4 The fluorescent tag mNeon green

mNeon green is a yellow-green fluorescent protein in monomeric form, which was originally derived from the tetrameric wild-type LanYFP found in the organism Branchiostoma lanceolatum (Shaner et al., 2013). With a high quantum yield (0.80 ± 0.016) and extinction coefficient (116 ± 4 mM-1cm-1) it exhibits the highest brightness of yellow or green fluorescent proteins yet described (Shaner et al., 2013). The excitation maximum of mNeon green lies at 506 nm, whereas the emission maximum can be found at 517 nm. According to the initial characterization of the protein by Shaner et al., it is suitable for single-molecule super-resolution imaging, as by using a high-power laser illumination it can temporarily be driven into a dark state. Further, it was argued to be ideal for FRET (Förster Resonance Energy Transfer), thanks to its high quantum yield and extinction coefficient (Shaner et al., 2013).

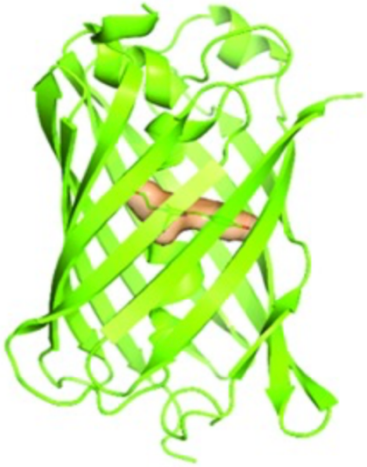

Figure 6 **mNeon green monomer** in crystals of space group P6522 obtained at pH 8.0

2. Aim of this thesis

The aim of this thesis is to bring forward new insight into the replication process of the avian reovirus, as the formation of inclusion bodies by the µNS protein play a fundamental role in it. Those inclusions are characterized by their liquid behaviour and assumed to be formed by liquid-liquid separation within the cytoplasm of the host (Broering et al., 2002).

Therefore, it was tried to produce a soluble µNS-mNeon fusion protein, which can then be purified and used as model for fluorescent observations of the formation of viral inclusion bodies. Further, this minimal in vitro model system should be suitable for detecting liquid-liquid phase separation driven by the µNS protein and solution conditions such as protein concentration, ionic strength and presence of complexing agents. This should then lead to the establishment of a phase diagram, which provides an overview of the conditions necessary to drive phase separation.

As the crystal structure of the µNS protein remains unsolved, several crystallization conditions were tested and the production of crystals suitable for X-ray diffraction and structural analysis was attempted.

3. Materials and methods

3.1 Transformation µNS-mNeon

To find the cell line most suitable for expression of µNS-mNeon, three different *E.coli* cells lines were tested and evaluated. To allow Affinity Chromatography, a N-terminal His Tag was present.

3.1.1 Into the competent *E.coli* cells BL 21 (DE3) (Invitrogen)

To transform the µNS-mNeon DNA into the competent cells, the frozen cell mixture BL 21 (DE3) C2527 (Invitrogen) was thawed on ice for 10 min before 1 µL of plasmid DNA: µNS_Cflex in pet 19b (Novagen) clone no.U1-6 (c=53.4 ng/µL) was added. In this step vortexing or ungentle mixing needed to be avoided to prevent the destruction of the cells. Incubation was performed for 30 min on ice and afterwards the cells were heat-shocked by putting the vial into a 42°C water bath for exactly 10 seconds and then back on ice for 5 min. Following, 250 µL of the to room temperature pre-heated SOC medium (New England Biolabs) was added, and the vial was put into the shaker for 60 min at 37°C and 225 rpm. To finish the transformation, 50 and 200 µL respectively of the reaction were spread onto selection plates containing ampicillin and incubated at 37 °C overnight.

3.1.2 Into competent *E.coli* cells BL21(DE3) CODON+

As expression of σNS in *E.coli* cells BL21(DE3) CODON+ (Agilent-RIPL), performed previously by the co-supervisor of this thesis, produced a higher yield of protein, it was considered to also use the CODON+ strain for µNS-mNeon.

For this cell type the transformation procedure was performed as described above. The only differences are in the duration of the heat shock, which lasted for 20 seconds and the incubation on ice for only two minutes.

3.1.3 Into competent E.cloni® EXPRESS cells

To get a third type for comparison, E.cloni® EXPRESS cells (Lucigen) were tested and used for expression.

After removing the cells from the freezer (-80°C) and thawing on ice for 10 min, 40 µL were transferred to a pre-cooled tube and 1 µL of plasmid DNA: µNS_Cflex in pet 19b (Novagen) clone no.U1-6 (c=53.4 ng/µL) was added. By gentle stirring with the pipette tip, the reaction was mixed and then incubated on ice for 30 min. The following heat shock was

performed for 45 seconds at 42°C and the tube was immediately returned to ice for 2 minutes. Then, 250 µL of the provided Expression Recovery Medium (heated previously to room temperature) were added and the vials were shaken at 37°C and 220 rpm for 60 min. Afterwards 50 and 200 µL were spread onto ampicillin containing plates and incubated overnight at 37°C.

3.2 Protein µNS / µNS-mNeon expression

To do either pilot expression or large-scale expression, the steps visualized in the following flowchart (Figure 7) were performed, whereby each was adapted according to the protocol of the specific cell line and plasmid. E.g. temperature during induction, induction chemical, time after induction.

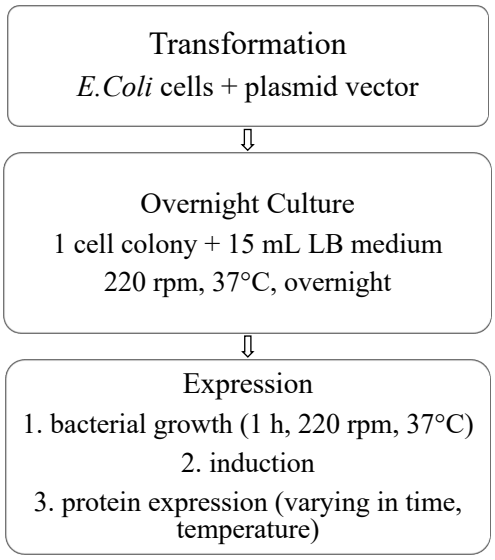

Figure 7 **general flowchart of protein expression**

3.2.1 Pilot expression

Preparation of overnight culture: In two 50 ml tubes respectively 15 ml of LB medium and 15 µL of the antibiotic Ampicilin (AMP; final concentration: 1 mg/mL) were mixed before one colony of the harvested cells was added to each one. Incubation was performed overnight at 37°C and 220 rpm.

Pilot expression: Next, 1 mL of the incubated medium was transferred to two new 50 mL vials containing 15 mL LB medium + AMP (final concentration = 1 mg/mL). After approximately 30 min, the OD_{600} was measured for the first time and after reaching a value of 0.5-0.6, IPTG was added (final concentration = 1mM) to induce protein expression. The flasks

were then put into separate shakers, whereby one was set to 30°C, 220 rpm and the other to 20°C, 220 rpm. Each hour 1 mL was taken, centrifuged at 12000 rpm for 1 min and the resulting pellet stored in the freezer. After 6 hours the cell expression was stopped and the taken samples analysed by SDS PAGE.

3.2.2 Large Scale Expression

Preparation of overnight culture: In four 50 ml tubes respectively 15 ml of LB medium and the 15 µL of the antibiotic AMP (final concentration= 1 mg/mL) were mixed before one colony of the harvested cells was added to each one. Incubation was performed over night at 37°C and 220 rpm.

Production: The following day, 200 mL of LB medium and 200 µL of AMP were mixed and the overnight cultures were added. After 1hour incubation at 37°C and 220 rpm further 600 mL of LB medium + AMP (1:1000) were poured into each bottle, to reach a total volume of 800 mL. After 30 min the OD_{600} was measured and as soon as the value lay between 0.5 and 0.6, induction was started by the addition of IPTG (for µNS-mNeon in pET 19b) or Anhydrotetracycline (for µNS in pASK-IBA37 plus) resulting in a final concentration of 1 mM IPTG or Anhydrotetracycline, respectively. Cell growth was then performed at 30°C and 220 rpm. Further, 1 mL of the sample was transferred to a new vial, centrifuged at 12000 rpm for 1 min and following the supernatant was discarded before storing the formed pellet of insoluble protein inside the freezer. This procedure was repeated each hour up to 4 hours and the vials were labelled accordingly and stored. After those 4 hours, the whole sample was centrifuged inside 1 L bottles at 4500 rpm for 30 min. Again, a cell pellet was formed, and the supernatant was removed until 30 mL of it remained. With this amount the pellet was resuspended and transferred to new tubes before centrifuging at 5000 rpm, 4°C for 20 min. Finally, the LB medium was discarded, and the cells stored at -80°C.

3.3 SDS-PAGE

Table 3 **SDS-PAGE gel preparation compositions**; separation gels (10%, 12.5%), stacking gel (4%)

separation gel	**12.5%**	**10%**
30% Acrylamide	2.08 mL	1.66 mL
H_2O	1.27 mL	1.98 mL
1.5 M Tris (pH=8.8)	1.25 mL	1.25 mL
10% SDS	50 µL	50 µL
10% APS	50 µL	50 µL
TEMED	5 µL	5 µL

stacking gel	**4%**
30% Acrylamide	340 µL
H_2O	1,36 mL
1 M Tris(pH=6.8)	250 µL
10% SDS	20 µL
10% APS	20 µL
TEMED	2 µL

Preparation of samples: After large scale expression the samples were again taken out of the freezer, thawed and resuspended by the addition of 500 µL lysis buffer (50 mM Tris, 500 mM NaCl, 5 mM MgCL2, 100 µg/mL DNase, 50 µg/mL RNase, proteinase inhibitor, pH 7.5) To facilitate lysis, a circle of 3 times freezing in liquid nitrogen and following thawing at 42 °C was performed. The samples were then centrifuged for 5 min at maximum speed and 4°C to allow the formation of a cell pellet containing the insoluble proteins. The remaining supernatant was transferred to a new vial and stored on ice, whereas to the insoluble pellet 500 µL of 1x SDS (125 µL 4x SDS, 375 µL PBS) was added. After cooling, 500 µL of supernatant were then mixed with an equivalent amount of 4x SDS (166.6 µL). Before boiling both the insoluble part and the insoluble protein at 95 °C for 5 minutes, the former was vortexed to guarantee resuspension of the pellet.

SDS-PAGE: The samples were then loaded onto the gel, which was prepared earlier according to Table 3. For comparison, 5 µL of PageRuler Protein Prestained Ladder (Thermo Fischer Scientific) was added to the first well of the gel. In the following wells the samples were loaded in the order of time points after induction with IPTG as well as the uninduced ones. The electrophoresis apparatus was then plugged in and the time was set for 1.5 hours.. After the first 30 min the voltage was increased from 100 V to 150 V and the electrophoresis proceeded. During this process, the parts were separated according to the size of proteins and with the help of the ladder, the protein in question could be identified later on gel. For this identification, the gel needed first to be taken out after finishing electrophoresis and submerged into Coomassie 250 Brilliant Blue (CBB) and placed on a shaker for 40 min. Secondly, the dye was discarded, and the gel was again put on a shaker for 1.5 hours while inside the de-staining solution (60% H_2O, 30% methanol, 10% acetic acid). After this treatment, the gel was analysed and a picture was taken.

3.4 Protein purification

Before each purification, the frozen cells needed to by lysed. This was achieved by first dissolving 1 pellet of protease inhibitor in 100 mL of lysis buffer (20 mM Tris, 400 mM NaCl, 5 mM $MgCl_2$; pH 7.0) and then adding 15 mL of the solution to each of the cell pellets. To disrupt the plasma membrane, the cells were first resuspended by vortexing and then passed through a French Press. The apparatus was afterwards washed with a small amount of lysis buffer to collect the complete sample. Next, 15 µL DNase (final conc. 10 µg/mL) and 15 µL RNase (final conc. 50 µg/mL) were added and incubated for 20 min at room temperature before the lysed cells were put into the ultracentrifuge (himac CP90WX - HITACHI) for 1 hour at 4°C and 40 000 rpm.

3.4.1 Immobilized metal affinity chromatography

This special type of chromatography allows a separation of proteins based on their affinity to metal ions. In this case, the ÄKTA Pure System (GE healthcare) was used, which was equipped with a HisTrap HP 5 mL column (GE Healthcare) containing Ni^{2+} ions, which further allow a purification of histidine containing proteins, such as the here used µNS mNeon construct.

Before purification was started the system needed to be first washed with ddH_2O (5 min, 5 mL/min) and then equilibrated using the following scheme (buffer composition in table 4):

- System pump: 5 min, 5 mL/min A-B-A
- Sample pump:1 min, 20 mL/min A

With a flowrate of 1 mL/min the sample was loaded onto the column and as soon as the UV started to rise rapidly, the collection of all not bound proteins was started into the outlet and marked as flowthrough (FT). By changing the tube back to the elution buffer, all remaining sample inside the tubes was pushed onto the column. As the UV had dropped to approximately 50 mAU, the first collection was stopped and elution from the column with 5% B was started. The UV again showed a sharp peak and the second collection proceeded until it dropped back to the baseline and a gradual increase to 100% of B within 20 min was set, which caused the collection of 1 mL fractions. After reaching this point, the fractionation was stopped, the fractions were transferred into dark 1.5 mL tubes, labelled and stored inside the fridge (4°C) for further use.

After each purification, the concentration of the collected fractions was determined by a spectrophotometer: extinction coefficient µNS-mNeon = 98835 (calculated by using the ProtParam tool; Gasteiger et al., 2005) molecular weight = 101.327 kDa

To prepare the system for another round of purification, it had to be equilibrated again as shown here:

- System pump: 5 min, 2 mL/min B
  10 min, 2 mL/min A
  5 min, 5 mL/min H_2O, both tubes
- Sample pump: 1 min, 20 mL/min H_2O
  1 min, 20 mL/min 20% EtOH
- Outlet: 1 min, 5 mL/min H_2O
- Fractionator: 30 sec, 5 mL/min H_2O

After equilibration and washing, all tubes were stored in 20% EtOH.

Table 4 **HisTrap** Equilibration buffer (A-left) + Elution buffer (B-right) composition

	A	B
Tris	20 mM	20 mM
NaCl	100 mM	100 mM
$MgCl_2$	7.5 mM	7.5 mM
Imidazole	-	1 M
pH	7.5	7.5

3.4.2 Anion exchange chromatography

This technique is based on the electrostatic interaction between two oppositely charged molecules. Here, the negatively charged proteins will bind to the positively charged resin beads loaded onto the column, whereas molecules with positive charged will flow through.

In this case, the ÄKTA Pure system (GE Healthcare) equipped with the HiTrap Q HP column (GE Healthcare) was used. Before starting to purify, the system was equilibrated as explained in the metal affinity chromatography. The procedure itself was performed as above, whereby elution started at 35% B (buffer composition in table 5) and fractions of 1 mL were collected, transferred into dark 1.5 mL tubes, labelled and stored inside the fridge (4°C) for further use.

After using, the column and the system were again washed, and the tubes were stored in 20% EtOH.

Table 5 **HiTrap**-Equilibration buffer (A-left) + Elution buffer (B-right) composition

	A	B
Tris	20 mM	20 mM
NaCl	100 mM	1 M
$MgCl_2$	7.5 mM	7.5 mM
pH	7.5	7.5

3.4.3. Size Exclusion Chromatography

In this process, the proteins should be separated based on their size. Smaller molecules are trapped in the pores of the stationary phase, whereas bigger ones can be easily eluted from the column.

This procedure was tried to obtain further purified μNS-mNeon protein using the ÄKTA Pure system (GE Healthcare) equipped with Superdex 200 Increase 10/350 GL column (GE Healthcare). After equilibration with ddH_2O and the buffer (20 mM Tris, 100mM NaCl, 7.5 mM $MgCl_2$, pH 7.5), fraction 4 from the previous Anion Exchange Chromatography was loaded onto the column using a pre-washed syringe. With a flowrate of 0.5 mL/min 100 μL fractions were collected after elution.

The following SDS PAGE showed no bands in the desired region and therefore it was concluded that the protein got stuck on the column and could not be further purified by this procedure.

3.4.4 Purification from Inclusion bodies

As also the insoluble fraction after ultracentrifugation showed the significant yellow-green of the fluorescent protein, it was considered for further experiments.

For that, the inclusion bodies first needed to be dissolved again by in a suitable buffer (6 M Guadinium Chloride, 20 mM Tris, 0.5 M NaCl, 5 mM Imidazole, 1 mM β-Mercapto-Ethanol; pH 7.5). After 24 h on the magnetic stirrer, the sample was ready to be loaded onto the HisTrap HP 5 mL column (GE Healthcare). The column was equilibrated with the equilibration buffer (20 mM Tris, 100 mM NaCl, 7.5 mM $MgCl_2$, 6 M Urea; pH 7.5) and elution started at approximately 20% of the elution buffer (20 mM Tris, 100 mM NaCl, 7.5 mM $MgCl_2$, 6 M Urea, 1 M Imidazole; pH 7.5). The collected fractions were then transferred

into dialysis tubing. Following, the tubes were placed into 2 L of dialysis buffer (20 mM Tris, 100 mM NaCl, 7.5 mM $MgCl_2$, 4 M Urea, 1 M Imidazole; pH 7.5) and the buffer exchange was performed on a magnetic stirrer in the cooling room. Over the next 2 days the buffer was consequently removed and replaced by first an equivalent with 1 M Urea and then with a buffer without any Urea.

After this procedure the sample was again purified on the ÄKTA Pure System (GE healthcare) with a HisTrap HP 5 mL column (GE Healthcare). The buffer compositions were as following: equilibration buffer = 20 mM Tris, 100 mM NaCl, 7.5 mM $MgCl_2$; pH 7.5, elution buffer = 20 mM Tris, 100 mM NaCl, 7.5 mM $MgCl_2$, 1 M Imidazole; pH 7.5. Fractionation was performed as above, the samples were put onto an SDS gel and then stored in 1.5 mL dark tubes at 4°C.

3.5 Western Blot

For confirming the presence of the wanted protein complex, analysis by western blot was performed.

First, SDS PAGE was done and afterwards the gel was blotted onto a Polyvinylidene fluoride (PVDF) membrane (Biorad), which was pre-incubated for 15 min in 100% Methanol and 15 min in 1xSDS transfer buffer (48 mM Tris, 39 mM Glycine, 1.3 mM SDS, pH 9-9.4). After incubating the gel and the filter papers in the transfer buffer, the blotting sandwich was assembled according to the Trans Blot Turbo (Biorad) Transfer Pack Quick Start Guide. The blotting lasted 30 min at 25 V and 1.0 A. After transferring the proteins from the gel, the membrane was washed 3 x 10 min in TBS-T (50 mM Tris, 150 mM NaCl, 0.1% Tween, pH 7.6) on a rocking station. Then the freshly prepared Blocking solution (5 mL 10x Blocking buffer (Qiagen), 0.5 g Blocking reagent (Qiagen), Tween 20 according to manufacturer) was added and blocking was done for 1 h at room temperature, before the membrane was again washed for 3 x 10 min in TBS-T. Following, the primary antibody (Penta His HRP Conjugate -Qiagen) was diluted 1:2000 in blocking solution and poured over the membrane. After 2 h incubation on a rocking platform at room temperature, the blocking solution was discarded, and the membrane washed for 2 x 10 min with TBS-T and for 1 x 10 min with TBS.

For staining, each 1 mL of Clarity Western ECL Substrates mix reagents in a 1:1 ratio were mixed, run over the membrane and incubated for 5 min before taking a picture.

3.6 Circular Dichroism

To evaluate whether the protein is folded correctly, a circular dichroism spectrum was measured and analysed. For that purpose, two samples after refolding dialysis were desalted, to avoid interferences with the measurement, and then 100 µL used. For baseline correction a buffer (20 mM Tris, 100 mM NaCl, 7.5 mM $MgCl_2$; pH 7.5) was taken as reference. With a bandwidth of 0.5 nm and 20 accumulations, the spectra between 195 and 260 nm was then recorded and the outcoming data was analysed.

3.7 Fluorescence Microscopy

Table 6 **a. Standard Composition of buffer** and **b. used PEG concentrations**

a.

Standard composition	
Tris	20 mM
NaCl	100 mM
$MgCl_2$	7.5 mM
PEG	x

b.

PEG 1000	**PEG 6000**	**PEG 10000**
20 mM	20 mM	20 mM
50 mM	50 mM	50 mM
100mM		

3.7.1 Preparation of buffers (PEG/NaCl):

50 mL of each PEG buffer were prepared based on the composition stated below (table 6). Overall 7 mixtures were made with different concentrations and molecular weights of the PEG. Table 7 also shows the different combinations of molecular weight and concentrations.

To further test the behaviour of the protein in different salt concentrations, six buffers varying in their composition were prepared. The concentration of Tris and $MgCl_2$ remained the same (20 mM Tris, 7.5 mM $MgCL_2$) in each 50 mL of buffer and the NaCl concentrations were as following: 0mM, 20 mM, 50 mM, 100 mM, 200 mM, 500mM.

All components from both PEG and NaCl buffers were prepared from their solid form by dissolving in ddH_2O and further pH was adjusted to 7.5 by using 37% HCl and vacuum filtration was performed.

3.7.2 Observation of liquid-liquid-phase-separated droplets

During all rounds of observations, following settings were used: 488 nm excitation beam, lowered laser intensity to approximately 20 % (this was adjusted depending on the visibility and amount of detected fluorescence, high intensities close to 100 % were avoided to not cause photobleaching). Further, the microscope was mostly set in a wide-field mode, but also total internal reflection (TIRF) was used to observe droplets, which were present in a region not more than 200 nm away from the coverslip surface.

The previously prepared NaCl and PEG buffers (composition in table 6, ratio in table 7) and the µNS-mNeon sample were then added to a removeable 12 Well Chamber (Ibidi). For each protein/buffer ratio from table 7, the complete set of NaCl and PEG concentrations was tested, respectively. This resulted in a total of 39 tested conditions. In the first round of experiments, the samples were observed immediately after addition of the protein. Then the sealed samples were stored at 4°C and the experiment was repeated over several days after the initial round. The same was done with the combination of µNS-mNeon and PEG buffers. Data in form of pictures was collected using the installed camera to establish an overview of how the viroplasms might change their appearance over time. Further, videos were taken to show the mobility of the droplets and to help distinguish between mobile droplets and static inclusions.

Table 7 **protein : buffer ratio**

protein	**NaCl**	**PEG**
20 µL	20 µL	-
20 µL	-	20 µL
20 µL	10 µL	-
20 µL	-	10 µL
10 µL	20 µL	-
10 µL	-	20 µL

After the first trials, a new production of µNS-mNeon was tested without any additional buffer. For this purpose, 30 µL of the protein in solution were added to each well of the chamber.

The same was done with fractions purified from inclusion bodies. Here, however, first only the protein by itself was observed and then the sample was treated with either NaCl or PEG. Observed changes were noted and discussed later.

3.8 Protein Crystallization

3.8.1 Pre-Crystallization Test

To determine the optimal sample concentration of µNS-mNeon in solution, a pre-crystallization test was performed using the PCT™ kit provided by Hampton Research and a 24-well plate adjusted for sitting drop vapor diffusion. Initially, 20 µL of each of the 4 reagents (A1, A2, B1, B2; compositions in table 8) were filled into the reservoir out of which 1 µL got transferred to the sample well, where it was mixed with 1 µL of the µNS-mNeon sample. The plate was then sealed and put to 4°C. After 20 min the wells were observed using a light microscope and evaluated by comparing it to a provided analysis guide (Hampton Research). Based on this, it was decided to proceed with the crystallization screening.

Table 8 **Pre-Crystallization Test** PCT™ kit; Hampton Research

Reagent A1	0.1 M TRIS Hydrochloride pH 8.5, 2.0 M Ammonium sulfate
Reagent A2	0.1 M TRIS Hydrochloride pH 8.5, 1.0 M Ammonium sulfate
Reagent B1	0.1 M TRIS Hydrochloride pH 8.5, 0.2 M Magnesium chloride hexahydrate, 30% w/v Polyethylene glycol 4,000
Reagent B2	0.1 M TRIS Hydrochloride pH 8.5, 0.2 M Magnesium chloride hexahydrate, 15% w/v Polyethylene glycol 4,000

3.8.2 Crystallization Screening

For crystallization two different approaches were performed. Once two 96-well plates with each 24 reservoirs were used in combination with the Crystal Screen HT™ by Hampton Research and the sample preparation was done by hand. A random set of conditions was chosen from the screen and 50 µL were pipetted into the reservoir. Following, four different protein : reagent ratios (1:1, 0.5:1, 1:0.5, 3:1) were pipetted into the wells.

Secondarily, 4 different screens (SG1 Screen, The Ligand Friendly Screen and Structure Screen 1+2; all provided by Molecular Dimensions; sample : reagent ratios in table s) were chosen and 50 µL of each reagent were transferred into the reservoirs of a "MRC" 2-Drop Plate (Douglas Instruments). The protein sample was then mixed with the reagent by the OryxNano robot (Automatic Protein Crystallization System; Douglas Instruments).

Table 9 **experimental set-up**; in µL

Name of Crystal Screen	**protein : reagent**	
SG1 Screen (Molecular Dimensions)	1:1	0.5:1
The Ligand Friendly Screen (Molecular Dimensions)	1:1	0.5:1
Structure Screen 1+2 (Molecular Dimensions)	1:1	0.5:1

4. Results

4.1 Production and Purification of soluble µNS-mNeon

As previous work on µNS-mNeon (done prior to this thesis) was successful in obtaining the protein in soluble phase, we started by testing different cell lines and transformation protocols to evaluate which would lead to the highest yield of expressed protein.

For the transformation of the pET 19 b Vector containing µNS-mNeon into competent *E.coli* cells BL21(DE3), induction was performed by adding IPTG to a final concentration of 1 mM and in time intervals of 1 hour a sample was taken and analysed by SDS PAGE. Figure 8 shows that 4 hours at 30 °C seem to be the most suitable induction time for a sufficient protein yield. In both the insoluble (resulting from the repeated freeze-thaw lysis of the whole cells; marked P) and soluble (marked S) fraction the desired band at 101 kDa could be detected by visualizing it with CBB following SDS PAGE.

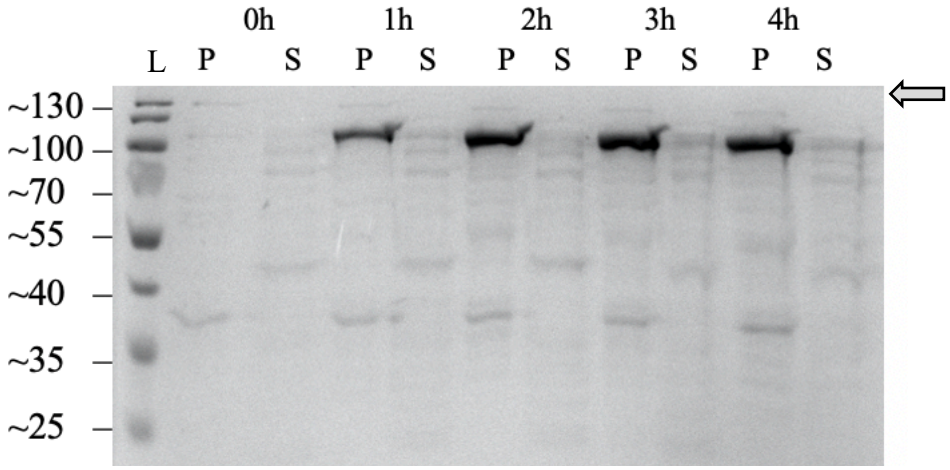

Figure 8 **SDS-PAGE of solubility test µNS-mNeon at 30 °C (12 µL)**
L- Prestained Protein Ladder (Thermo Fischer)
P- cell pellet
S- supernatant
0h-4h time after induction with 1mM IPTG

After transformation of the plasmid pET 19b Vector containing µNS-mNeon into competent *E.coli* cells BL21(DE3) CODON+ (agilent-RIPL), the cells were again induced with IPTG (final concentration 1 mM) and protein expression took place at 30 °C for 4 hours. Analysis with SDS PAGE (Figure 9) revealed an optimal induction time of 3h and it was decided to proceed with this experimental set-up in the following work.

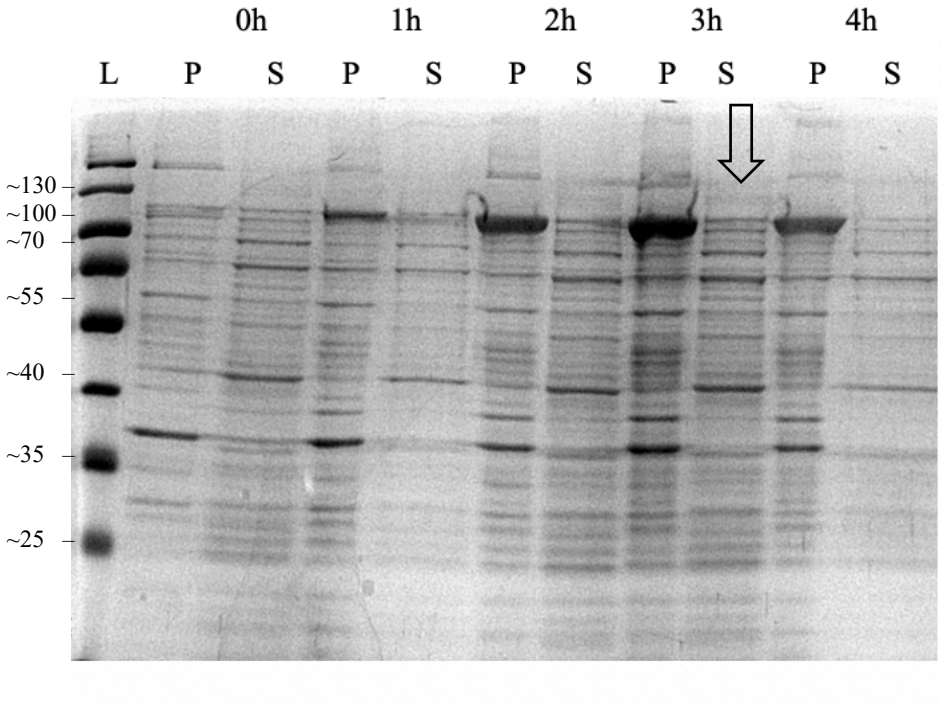

Figure 9 **SDS-PAGE of solubility test µNS-mNeon in Codon+ (RIPL-agilent) at 30°C (12 µL)**
L- Prestained Protein Ladder (Thermo Fischer)
P- cell pellet
S- supernatant
0h-4h time after induction with 1mM IPTG

By analysis with SDS-PAGE and comparison of the outcome of the different cell types, concerning the protein yield after pilot expression and further purifications, as well as visual assessment of the distinctive yellow-green colour of the fluorophore mNeon (already visible after production) it was decided to use competent *E.coli* cells BL21(DE3) CODON+ (agilent - RIPL) for future productions.

As it can be seen in figures 8 and 9, the sample needed to be purified further to obtain a purer solution of µNS-mNeon, which could be used in the next steps. Therefore, purification using the ÄKTA Pure system (GE Healthcare) equipped with the HisTrap HP 5 mL column (GE Healthcare) was performed. In cases, where this first round of purification did not lead to a satisfactory purity of the protein, an additional Anion Exchange Chromatography (ÄKTA Pure system with a HiTrap QHP 5 mL column (GE Healthcare)) was done. The results of both such procedures were analyzed by SDS PAGE, visualized using CBB staining and documented below.

Figure 10 depicts the typical outcome of metal affinity chromatography using a column charged with Ni^{2+} ions. The expected bands at 101 kDa are clearly visible, however, many other contaminants, in comparably high amount, are still present. Thus, a further purification was needed. To decide which fractions would be most suitable for such a procedure, the purity

of the sample was weighed against the protein concentration. At this point it has to be mentioned, that it was tried to achieve the highest protein concentration possible, so more importance was put to the amount of protein. Those fractions with high purity but low concentration were used directly for following fluorescence experiments, without any further purification steps.

The respective chromatogram from the affinity chromatography is shown in right panel of Figure 10 The second peak shows the collected fraction and it can be seen that contrary to the first peak (FT), the amount of protein (UV_280) is higher than the one of nucleic acids (UV_260).

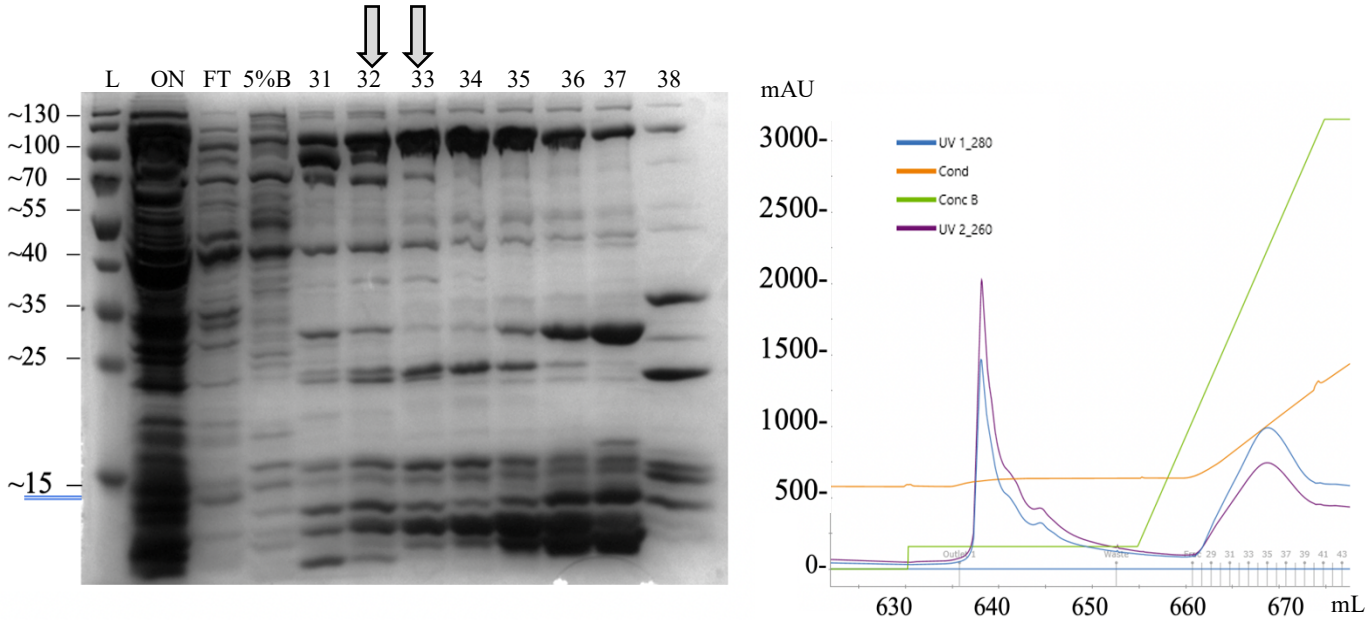

Figure 10 **SDS-PAGE of Affinity Chromatography purification µNS-mNeon (12 µL)** and **Chromatogram of IMAC purification µNS mNeon**
L- PageRuler Prestained Protein Ladder (Thermo Fischer)
ON- loaded sample
FT- flow through prior to elution
5%B- fraction after using 5% of buffer B
31-38 eluted fractions

UV 1_280	protein
UV 1_260	nucleic acids
Conc B	concentration of elution buffer B
Cond	conductivity

Following, fractions from the previous HisTrap purification with high concentration but rather low purity (see fractions 33 and 34 from Affinity Chromatography) where subsequently purified with the help of Anion Exchange Chromatography to obtain a sufficient yield of protein in the sample as well as no additional impurities (see fraction 3 from Figure 11).

The below depicted chromatogram already indicates a high yield of protein, as a high and sharp peak in the UV trace was observed when collecting the fractions. Further, the protein to nucleic acid ratio is rather large (A280 : A260 >2), suggesting a good purity of the sample.

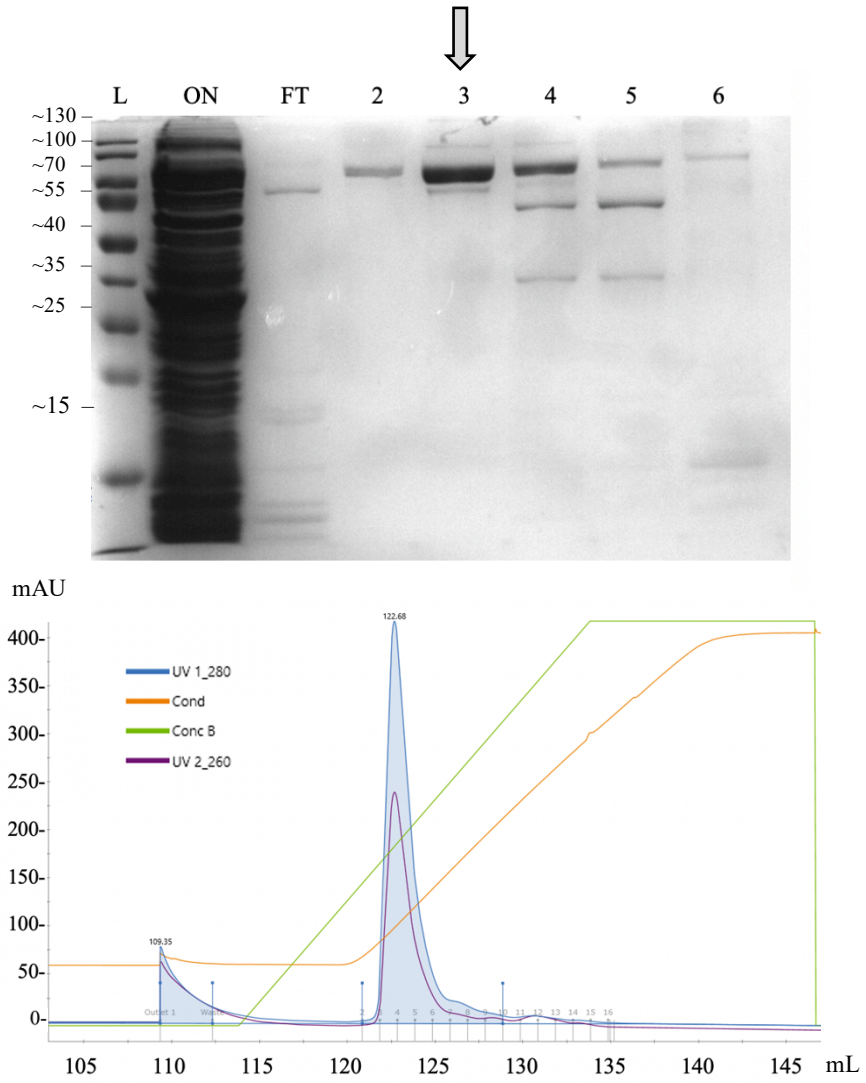

Figure 11 **SDS-PAGE of Anion Exchange Chromatography purification µNS-mNeon (12 µL) and Chromatogram of IMAC Anion Exchange purification µNS mNeon**
L- PageRuler Prestained Protein Ladder (Thermo Fischer)
ON- loaded sample
FT- flow through prior to elution
2-6 eluted fractions

UV 1_280	protein
UV 1_260	nucleic acids
Conc B	concentration of elution buffer B
Cond	conductivity

In some cases, however, we could generate sufficiently pure samples already from a single round of purification by Affinity Chromatography. The shown gel (Figure 12) obtained after SDS PAGE and staining with CBB shows such an outcome (protein concentrations: 6 – 1.3 mg/mL; 7- 1.9 mg/mL; 8- 1.5 mg/mL).

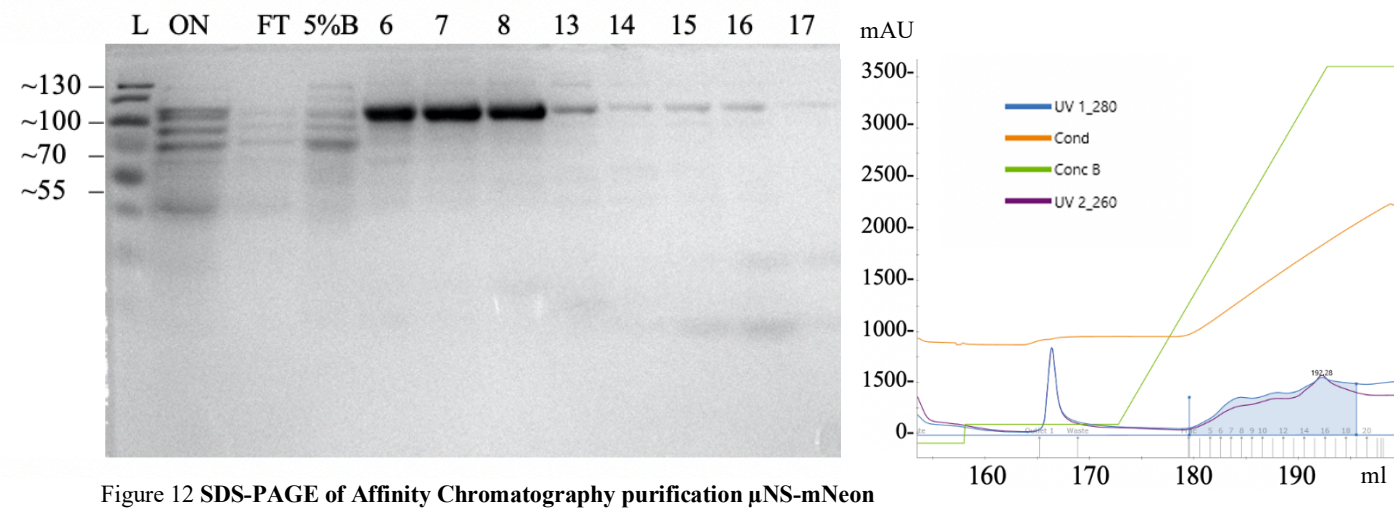

Figure 12 **SDS-PAGE of Affinity Chromatography purification µNS-mNeon (12 µL)**
L- Prestained Protein Ladder (Thermo Fischer)
ON- loaded sample
FT- flow through prior to elution
5%B- fraction after using 5% of buffer B
6-8, 13-17 eluted fractions

UV 1_280	protein
UV 1_260	nucleic acids
Conc B	concentration of elution buffer B
Cond	conductivity

4.2 Purification of µNS-mNeon from the insoluble fraction

As the protein µNS-mNeon complex seemed to be also present in the insoluble fraction obtained after ultracentrifugation (based on the yellow-green colour), those parts were dissolved again in a suitable buffer (6 M Guadinium Chloride, 20 mM Tris, 0.5 M NaCl, 5 mM Imidazole, 1 mM β-Mercapto-Ethanol; pH 7.5) and then purified under denaturing conditions (20 mM Tris, 100 mM NaCl, 7.5 mM $MgCl_2$, 6 M Urea; pH 7.5), using the ÄKTA Pure system (GE Healthcare) equipped with the HisTrap HP 5 mL column (GE Healthcare). Figure 13 shows the SDS PAGE after staining with CBB and it can be seen that the obtained fractions (4-13) contained µNS mNeon in significant amounts. The protein collected from fractions 7-10 were then refolded by dialysis and used for observation under the fluorescent microscope.

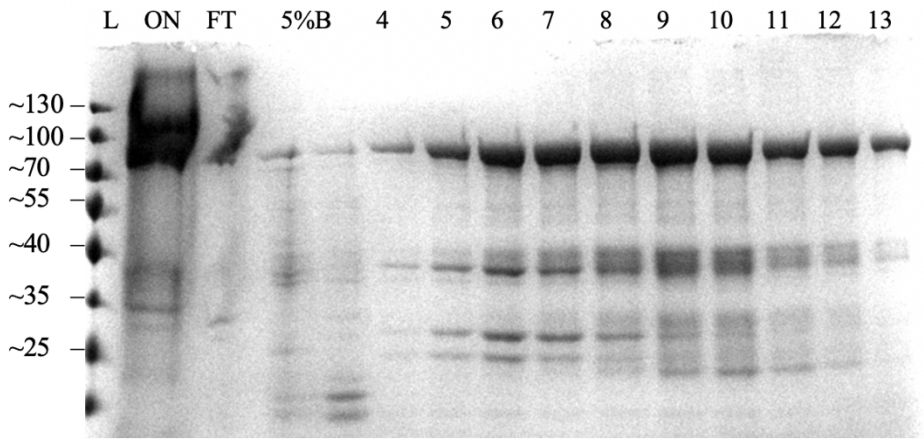

Figure 13 **SDS-PAGE of Affinity Chromatography purification µNS-mNeon from inclusion bodies (12 µL)**
L- Prestained Protein Ladder (Thermo Fischer)
ON- loaded sample
FT- flow through prior to elution
5%B- fraction after using 5% of buffer B
4-13 eluted fractions

To verify, whether the protein is truly present in the sample, Western Blot using the Trans Blot Turbo (Biorad) system was performed. This was achieved by detecting the N-terminal His Tag using a Penta His HRP Conjugate (Qiagen) antibody. The shown PVDF membrane in figure 14 a. visualizes a band at 101 kDa and therefore suggesting the presence of the µNS-mNeon complex. By comparison of the PVDF membrane with the respective gel from SDS PAGE (Figure 14 b.) , stained with CBB, this assumption could be confirmed.

At this point we were not able to say, whether the bands seen in the lower regions were contaminations coming from a smaller protein, or proteolytic fragments, which also had an His Tag attached.

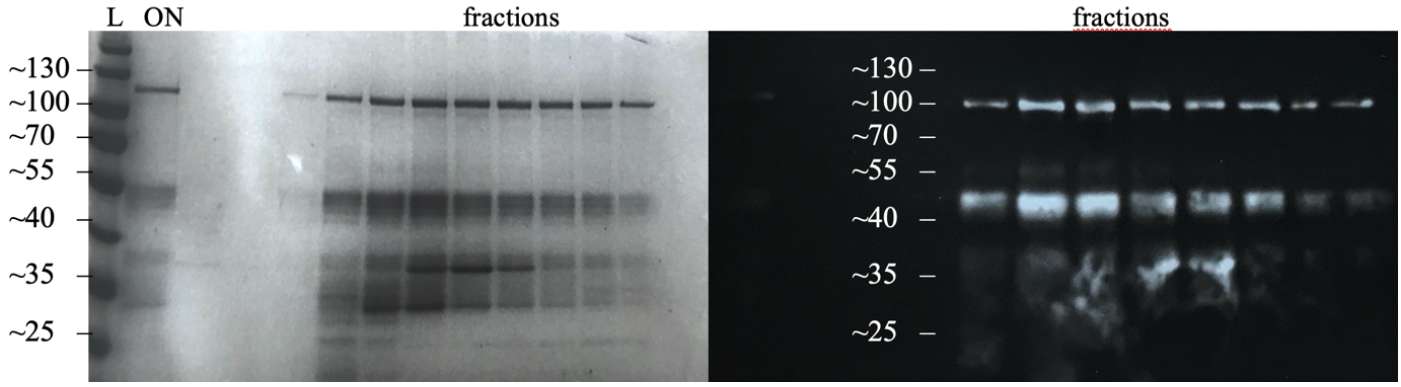

Figure 14 a. **SDS PAGE µNS-mNeon (10 µL)** b. **Western Blot µNS-mNeon**
L- Prestained Protein Ladder (Thermo Fischer)
ON- loaded sample

As a verification technique whether the protein is folded correctly and present in its expected structure, a CD measurement was performed and analyzed. Figures 16 and 17 show the obtained spectra. It can be clearly seen that the signal detected was rather low, when compared to the standard spectra (Figure 15) used as a reference. However, both spectra exhibit some local maxima and minima at distinct wavelengths. When looking at the standard spectrum of a α-helix , two minima at closely after 220 nm and at around 208 nm and a shallow maximum at approximately 215 nm can be seen. Despite their rather low amplitude, all three of those points can also be observed in the two measured spectra and therefore it was concluded that most of the protein must be present in α-helices. However, the shoulder minimum at 218 nm is evident for the presence of a beta-sheet, which was expected based on the structure of mNeon (Figure 6). For comparison, the spectrum of GFP (Figure 18) was chosen, as this fluorescent protein shows identical folds and similar properties.

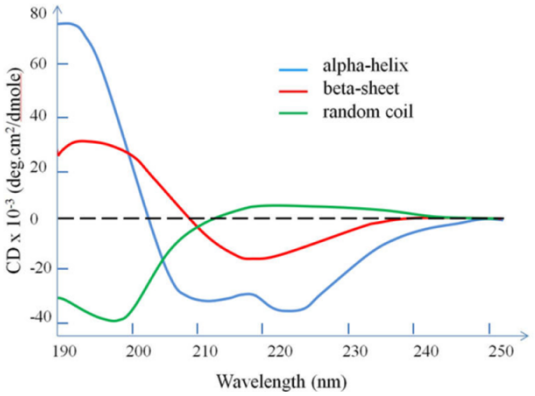

Figure 15 **standard CD spectrum**

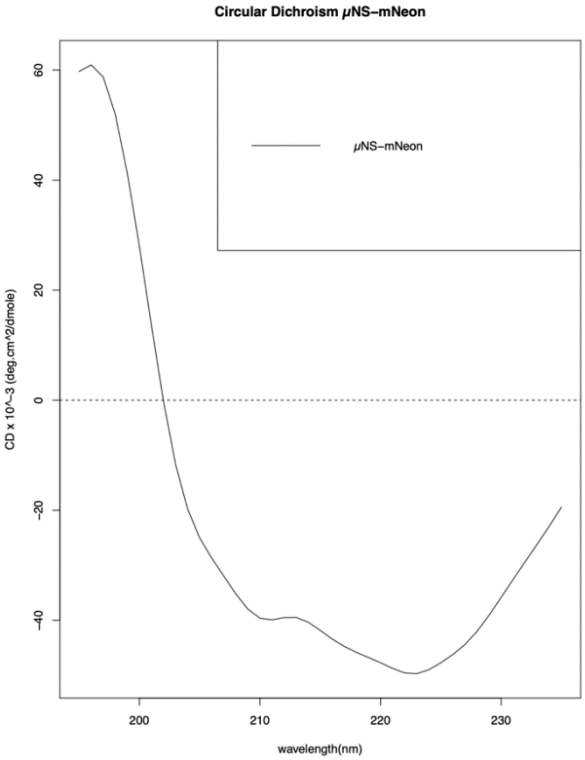

Figure 16 **CD spectrum µNS-mNeon soluble fraction**

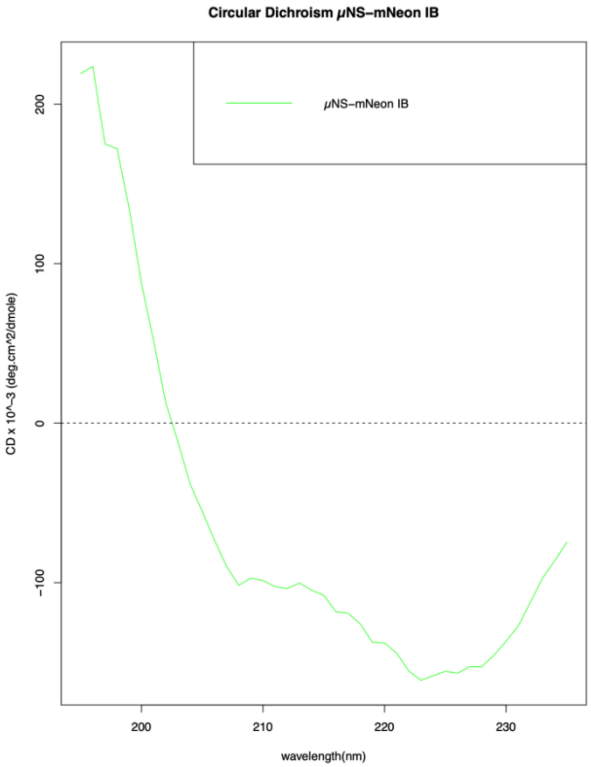

Figure 17 **CD spectrum µNS-mNeon purified from inclusion bodies**

Based on results from the CONTIN program, the secondary structure is built from a majority (52± 2 %) of beta-sheets (Visser, Hink, Borst, van der Krogt & Visser, 2002), which are forming a beta-barrel, just as the mNeon protein.

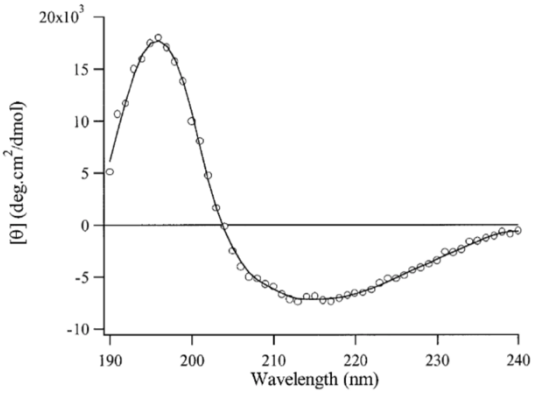

Figure 18 **CD spectrum of GFP** (Visser, Hink, Borst, van der Krogt & Visser, 2002),

4.3 Observation of viroplasms under the fluorescence microscope

After purification of µNS-mNeon and analysis of the fractions by SDS PAGE, the concentration of each sample was measured with a spectrophotometer. A representative group of samples with a range of protein concentration (initial: 0.5 mg/mL – 4.5 mg/mL) was chosen and used for fluorescence experiments.

The first round of observations showed to be very successful, as already immediately after adding the protein sample, purified using a HisTrap HP 5 mL column (20 mM Tris, 100 mM NaCl, 7.5 mM $MgCl_2$, 1 M Imidazole; pH 7.5), bright, mobile and globular spots could be detected (Figure 19 a.). By increasing the amount of salt concentration in the additional buffer (20 mM Tris, (0-500) mM NaCl, 7.5 mM $MgCl_2$; pH 7.5) it was tried to cause a change in either general formation, shape and amount of viroplasms. Figure 19 a.-f. show different conditions and the respective outcome. It can be seen that the formed droplets only vary slightly in size and appear to be very similar in shape.

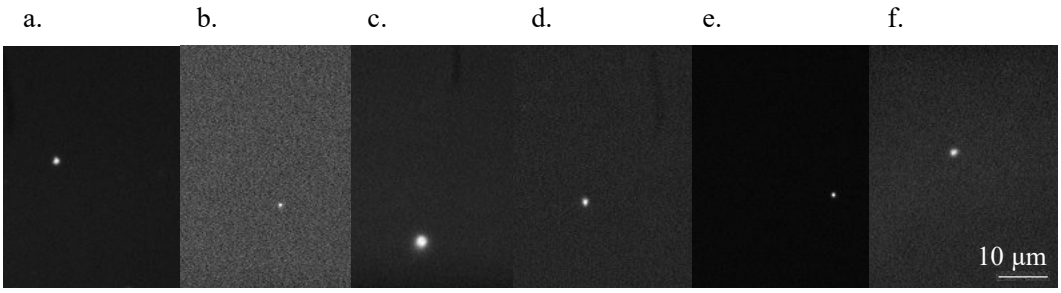

Figure 19 **µNS-mNeon viroplasms immediately after buffer addition**
a. 0.465 mg/mL protein in 0 mM NaCl; **b.** 0.465 mg/mL protein in 20 mM NaCl; **c.** 0.465 mg/mL protein in 50 mM NaCl; **d.** 0.465 mg/mL protein in 100 mM NaCl; **e.** 0.465 mg/mL protein in 200 mM NaCl; **f.** 0.465 mg/mL protein in 500 mM NaCl
(Note: protein concentrations are final concentrations; same magnification in a.-f.)

Figure 20 shows the summary of tested protein and salt concentrations (immediately after protein addition) The samples, in which droplet formation was detected, are marked blue, those, in which none were found, are marked orange. The number of droplets observed per field of view is visualized by differently sized data points. It can be seen that globules were formed in a majority of conditions and those positive results are spread over a wide concentration range of both protein and NaCl.

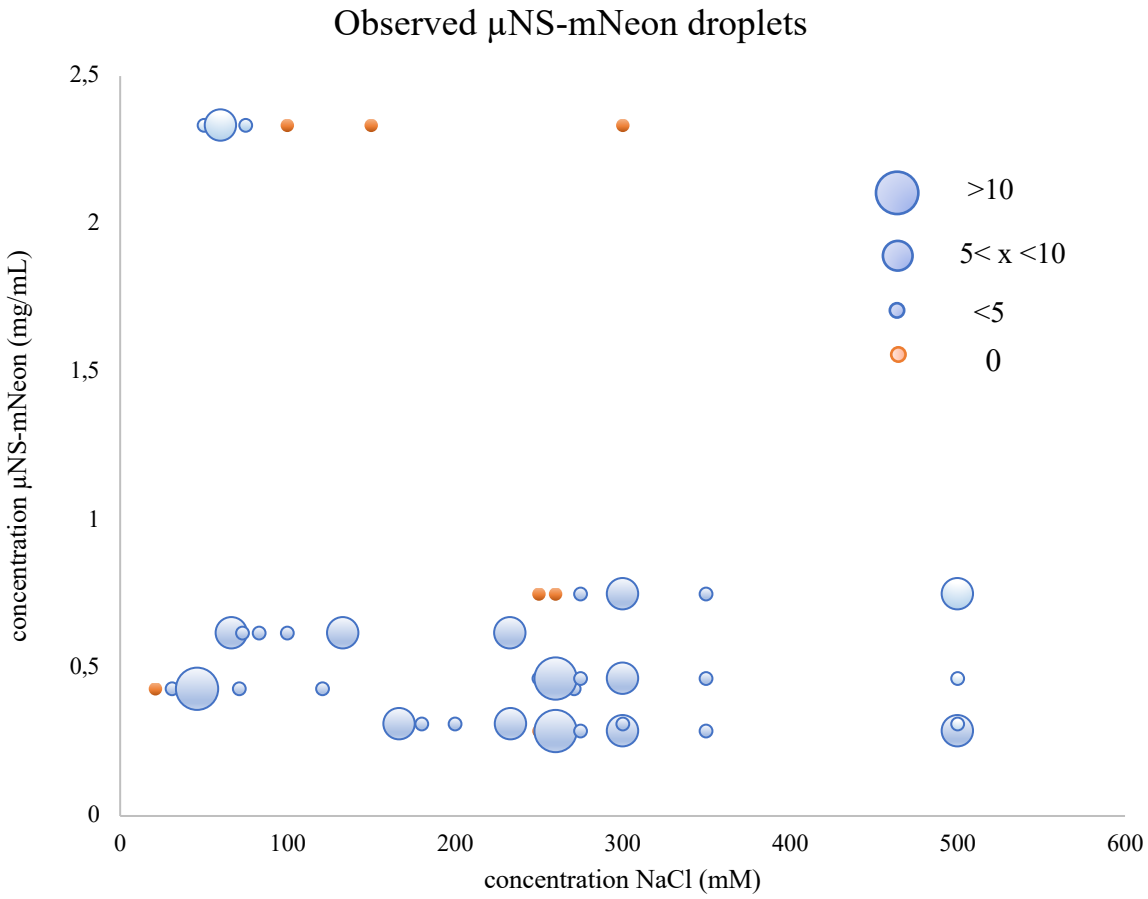

Figure 20 **Observed µNS-mNeon droplets** over a range of protein and NaCl concentrations; blue – droplets were observed; data point size indicates number of observed droplets per field of view ; orange – no droplets visible

Further, in those samples, where droplets could be detected, it was counted how many spots were visible in the field of view and how often this number occurred in different conditions salt conditions (Table 10, Table 11) The protein concentration in all samples of table 10 was 0.465 mg/L and 2.330 mg/L in table 11. Figure 22 a.-f. further visualize these observations (only including results from table 10).

It can be seen, that in conditions with a lower amount of NaCl added (0 mM, 20 mM, 50 mM) the number of viroplasms observed ranged between 1 and 6 (except the outlier of 10 in the 20 mM sample). In contrast, in samples treated with higher concentrations of NaCl (100 mM, 200 mM, 500 mM) the number of observed droplets rose up to 14. However, in a number of samples, no matter the NaCl condition, no droplets were detected. Furthermore, in the samples treated with an additional 200 mM NaCl buffer, higher (10, 14), but also lower (1, 5) number of droplets were observed per field of view (Table 10; Figure 22 e.). Figure 21 gives a visual representation of those observations made in higher salt environments.

Table 10 **number of observed droplets**; per field of view and depending on NaCl concentration. Final protein concentration = 0.465 mg/L

NaCl added	number of droplets (per field of view)	observed times
0 mM	0	2
	1	5
	4	1
	6	1
20 mM	0	2
	1	3
	3	3
	10	1
50 mM	0	3
	1	3
	2	2
	3	1
100 mM	0	3
	2	3
	3	1
	6	1
	7	1
200 mM	0	1
	1	3
	5	1
	7	1
	8	1
	10	1
	14	1
500 mM	0	1
	1	1
	2	2
	8	2

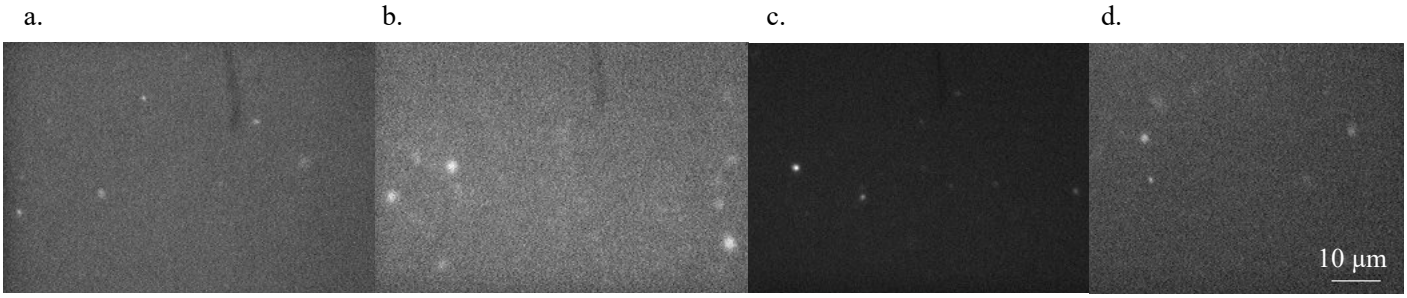

Figure 21 **µNS-mNeon globules at higher NaCl conditions**
a. 500 mM NaCl; **b.** 200 mM NaCl **c.** 200 mM NaCl; **d.** 500 mM NaCl
(Note: same magnification in a.-d.)

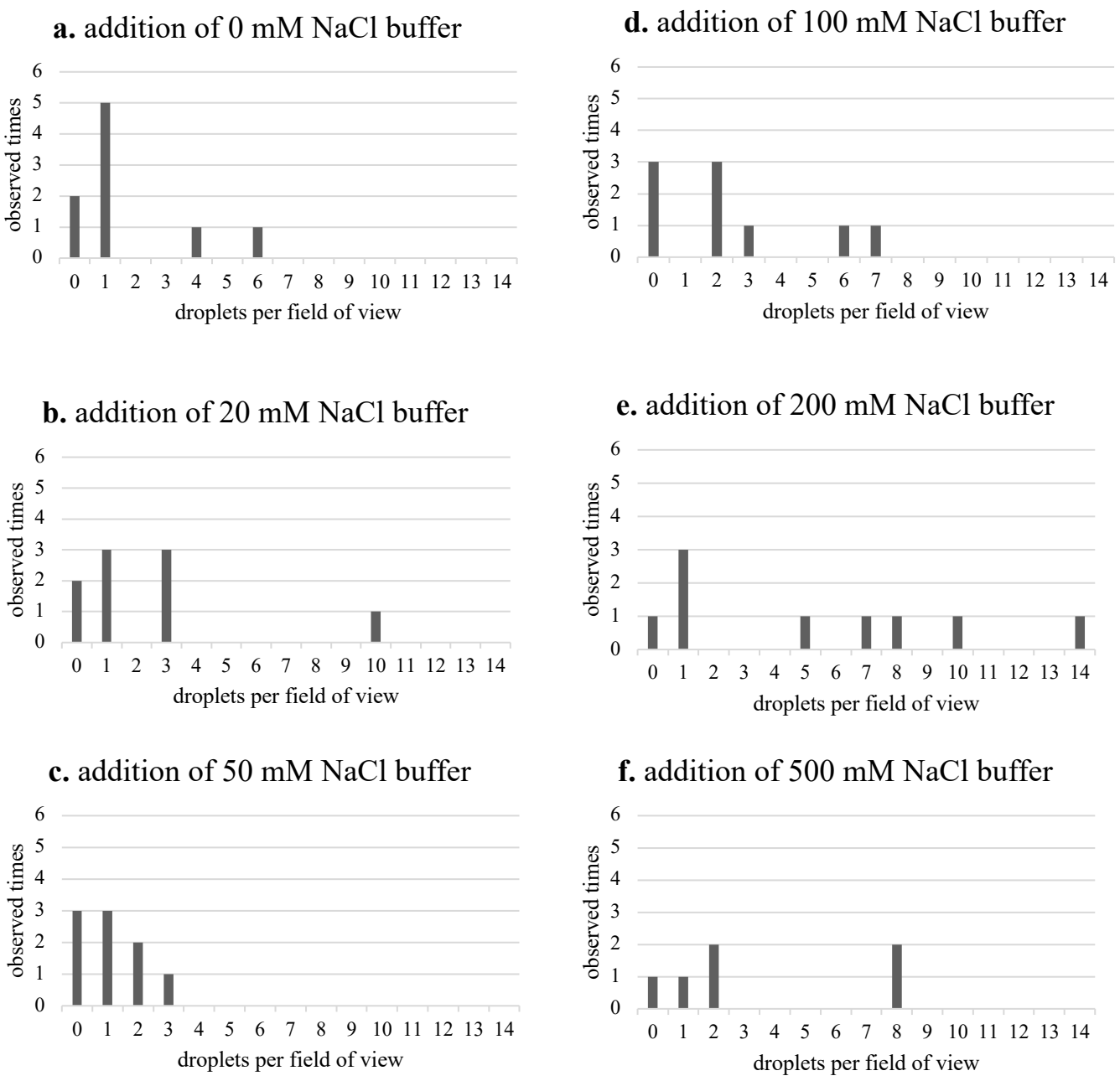

Figure 22 **Observed µNS-mNeon droplets per field of view** in a series of NaCl conditions. (final protein concentration = 0.465 mg/mL).
a. 0 mM NaCl buffer added **b.** 20 mM NaCl buffer added **c.** 50 mM NaCl buffer added **d.** 100 mM NaCl buffer added
e. 200 mM NaCl buffer added **f.** 500 mM NaCl buffer added

When analyzing the observation results of the higher protein concentration sample (2.330 mg/L; Table 11), it can be seen, that in those samples treated with higher salt concentrations (100, 200, 500 mM), no droplets were detected. This is in contrast to the lower protein sample (0.465 mg/L; Table 10), in which the occurrence of droplets seems to increase upon addition of buffers with higher salt concentration. Finally, it has to be noted, that as no droplets appear to have formed at higher salt conditions, it was decided during the experiments to continue with the lower protein concentration samples. Thus the inequivalence in the number of total observations.

Table 11 **number of droplets observed**; per field of view and depending on NaCl concentration. Final protein concentration = 2.330 mg/mL

NaCl added	number of droplets	observed times
0 mM	0	1
	1	2
	5	1
20 mM	0	2
	3	2
50 mM	0	2
	2	2
100 mM	0	4
200 mM	0	4
500 mM	0	4

The samples were then sealed and stored at 4°C, to repeat observations 1 day, 2 days and 3 days after the initial round. Figure 23 shows a representative group (protein concentration = 0.456 mg/mL; NaCl concentration of the buffer = 0 mM) of the obtained results. It can be seen that the visual appearance of the droplets did not change over time and the below pictured globules were still mobile.

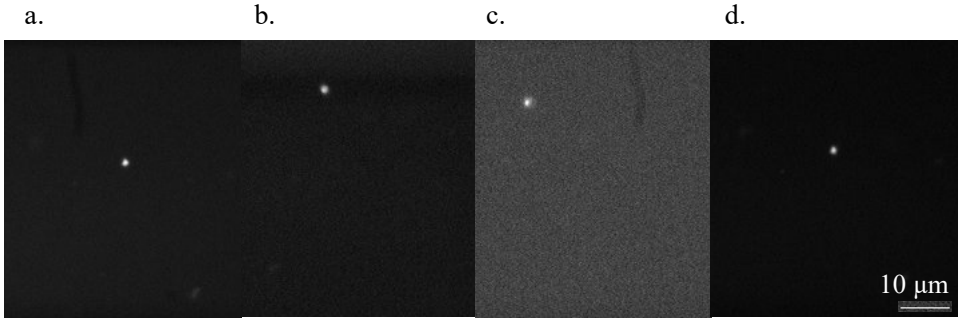

Figure 23 **µNS-mNeon (0.456 mg/mL) globules over time in a 0 mM NaCl buffer**
a. immediately after addition; **b.** 1 day later; **c.** 2 days later; **d.** 3 days later
(Note: same magnification in. a.-d.)

When looking at the same sample treated with the PEG buffer, the result showed to be very similar to what had been observed in the protein-NaCl buffer combination (compare Figure 19 and 24 a.-b.). However, some differences could be seen, such as the amount of detected aggregation. While after adding the NaCl buffer, in most samples the inclusions were present in an otherwise "clear" solution, a higher amount of irregular shaped aggregates was detected in samples with additional PEG. Especially at higher concentrations or higher molecular weight (Figure 24 c. and d.) this phenomenon occurred.

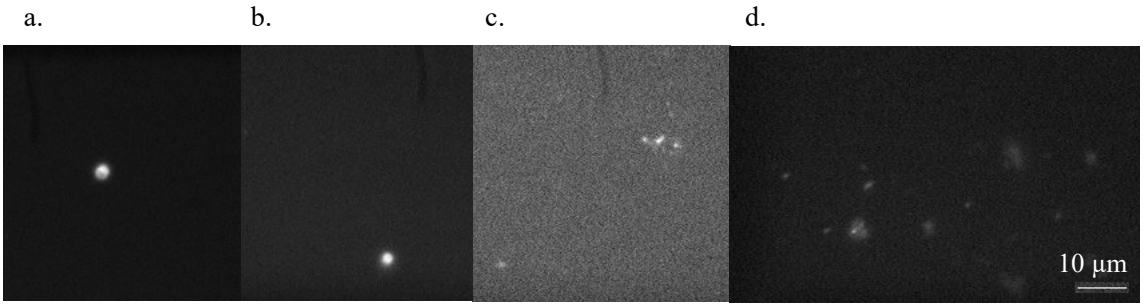

Figure 24 **µNS-mNeon globules in PEG**
a. 0.465 mg/mL protein in 20mM PEG1000; **b.** 0.465 mg/mL protein in 50mM PEG6000; **c.** 0.465 mg/mL protein in 20mM PEG10000; **d.** 0.465 mg/mL protein in 50mM PEG10000
(Note: protein concentrations are final concentrations; same magnification in a.-d.)

As mentioned earlier, we were able to obtain significant amounts of µNS-mNeon after purification from inclusion bodies (Figure 13) and therefore observed the samples under the fluorescent microscope to verify whether or not viroplasm formation was also present here. For that purpose, fraction 8 (Figure 13) was used. However, SDS PAGE analysis already revealed several other bands in regions of lower molecular weight, possibly indicating impurities. We then encountered these impurities again during fluorescent experiments, where they were seen as either static or free-flowing irregularly shaped aggregates (Figure 25). Some exhibited fluorescence, while others did not show any of such behavior. The process of purifying from inclusion bodies was later repeated several times followed by observations under the fluorescence microscope. In some cases, globular and fluorescent particle were detected, however, the majority of samples still contained a high amount of impurities.

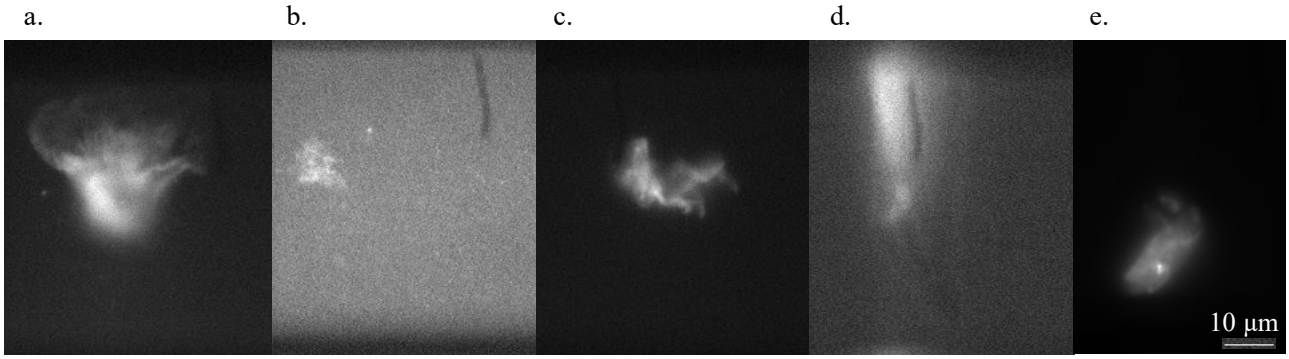

Figure 25 **aggregates of µNS-mNeon**
a. 0.465 mg/mL protein in 250 mM NaCl; **b.** 0.465 mg/mL protein in 275 mM NaCl; **c.** 0.465 mg/mL protein in 500 mM NaCl; **d.** 0.465 mg/mL protein in 350 mM NaCl; **e.** 0.465 mg/mL protein in 275 mM NaCl
(Note: protein concentrations are final concentrations; same magnification in a.-e.)

Lastly, the size distribution depending on the NaCl concentration was analyzed by first converting the measured pixel size to the droplet diameter in µm and then plotting those results against the number of times a specific diameter range was observed. For that, the same pictures as those used for establishing table 10 and figure 22 were used (final protein concentration = 0.465 mg/mL). Figure 26 a.-f. illustrate the obtained results (Note: different scaling of the y-axis in **e.** due to a higher number of observed droplets). In most conditions (0 mM, 20 mM, 100 mM, 200 mM) the majority of droplets had an approximate diameter between 0.80 and 1.19 µm. Also in the 500 mM NaCl conditions, the 0.80 – 1.19 µm range was observed eight-times and only the 1.20 – 1.59 µm diameter range was observed more often (ten-times). The results of the 50 mM NaCl conditions, however, do not follow this trend and the size distribution is spread rather evenly over the range of 0.80 to 3.59 µm. Additionally, the range of 3.20 – 3.59 µm was only reached here, while in the other tested NaCl condition, the maximum value ranged between 1.59 and 2.39 µm. The smallest diameters (0.01 – 0.39 µm) were found in the 20 mM and 200 mM salt environments.

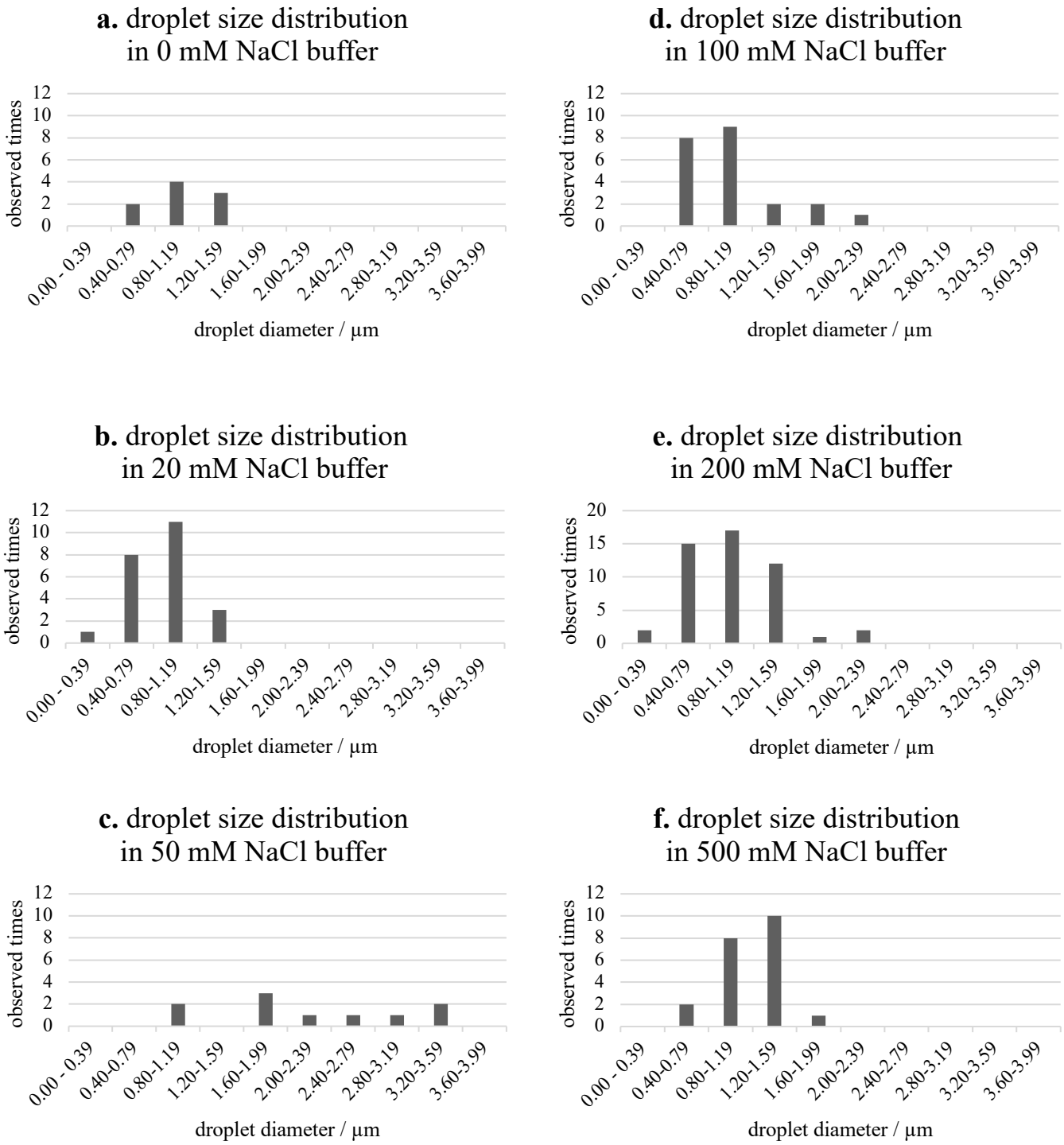

Figure 26 **Size distribution (as droplet diameter given in µm) of observed µNS-mNeon droplets** in a series of NaCl conditions.
a. 0 mM NaCl buffer added **b.** 20 mM NaCl buffer added **c.** 50 mM NaCl buffer added **d.** 100 mM NaCl buffer added
e. 200 mM NaCl buffer added (Note: different scaling of the y-axis in e. due to a higher number of observed droplets).
f. 500 mM NaCl buffer added

4.4 Crystallization of µNS-mNeon

As we were able to obtain well-folded µNS-mNeon in sufficient quantities (>1mg/mL; see section 4.1 and 4.2), it was attempted to produce protein crystals suitable for X-ray crystallography and subsequent 3D structure determination.

After the initial pre-crystallization test revealed a sufficiently high concentration of protein in the sample, various crystallization screens were used for screening. Following a one-week growth period, the drops were observed. Most did not show any crystal formation and were clear and some developed light or partly heavy precipitate. However, in a small number of conditions we could detect crystals, which were either of protein or salt origin. To distinguish between those two options, the polarizing filter of the light microscope was used.

Based on that, single crystals were harvested and measured on Synchrotron Radiation at BESSY II in Berlin (this part was performed by a different lab group, which was working on several other crystals at the same time). Figure 27 a.-c. show three different crystals grown under different conditions. In c. a light green coloration can be seen, which indicates the presence of the mNeon green protein. However, the shown crystals did not diffract.

a. b. c.

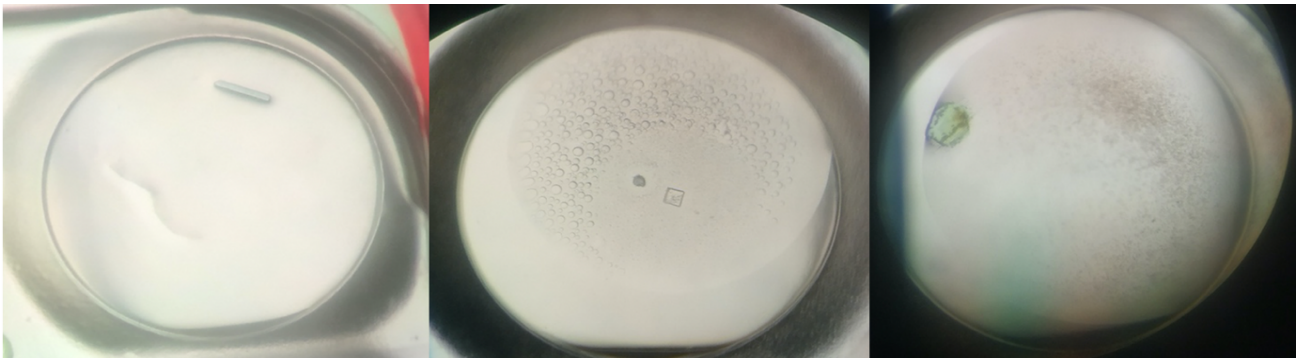

Figure 27 **Crystallization Screening**
a. Structure Screen 1+2 HT-96 (Molecular Dimensions): 0.2 M lithium sulfate, 0.1 M Tris, pH 8.5, 30 % w/v PEG 4000, µNS-mNeon 1 mg/mL
b. MIDASsplus HT-96 (Molecular Dimensions) : 0.1 M Tris, pH 8, 30 % w/v Poly(acrylic acid sodium salt) 5100 +hexanediol, µNS-mNeon 1.18 mg/mL
c. Structure Screen 1+2 HT-96 (Molecular Dimensions): 0.1 M Tris, pH 8.5, 2.0 M ammonium sulfate, µNS-mNeon 1 mg/mL

Further attempts of crystallizing µNS-mNeon were later performed by using different crystal screens and conditions. As this was done at the end of time dedicated to this thesis, the grown crystals were only observed under a light microscope and respective pictures are presented in figure 28 a and b. Here, we have two examples which could be from protein origin, as they did not change colour under a polarizing. Further, their shapes were compared to an observation guide (Hampton Research), which supported the presence of protein crystals. Figure 28 a. shows many small, unregularly shaped ("Whiskers", needle clusters) and seemingly linked crystals and in Figure 28 b. so-called crystal-needles can be seen. Both of these are rather unsuitable for structure determination, due to their shape and size and therefore, no further attempts to verify the presence of protein crystals were performed and as in most other conditions mainly salt crystals were formed, the process still needs to be optimised in future to obtain useable crystals.

a. b.

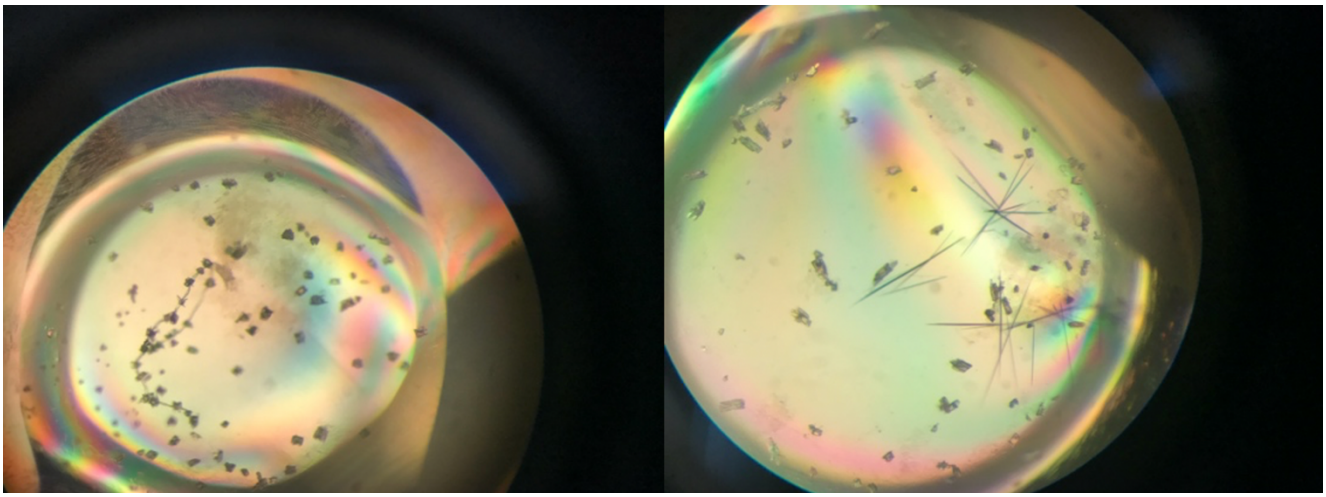

Figure 28 **Crystallization Screening**
a. Crystal Screen: 0.01 M Nickel (II) chloride hexahydrate, o1. M Tris pH 8.5 1.0 M Lithium sulfate monohydrate; 1:1 µNS-mNeon 1 mg/mL
b. Crystal Screen: 0.01 M Nickel (II) chloride hexahydrate, o1. M Tris pH 8.5 1.0 M Lithium sulfate monohydrate; 0.5:1 µNS-mNeon 1 mg/mL

5. Discussion

To visualize phase separation, the fluorescent tag mNeon was attached to the µNS protein (construct already present prior to this thesis). After initial expression in *E.coli* competent BL21(DE3) cells (Invitrogen), it was decided to proceed with the Codon+ cells by agilent-RIPL, as these generated a higher protein yield, combined with faster cell growth (Figure 9). A third cell line (E.cloni® EXPRESS cells (Lucigen)) was tested, but after unsuccessful transformation, not used any further.

After purification and first fluorescence experiments, the changes in shape and amount of the inclusions were assessed over several days and the results were tabulated to quantify under which conditions phase separation takes place. As it can be seen in figure 19, viroplasm formation was already observed immediately after addition of the respective buffer, and those visual observations concerning the globular shape differed only insignificantly in the different conditions. When looking at table 10, it could be concluded, that a higher concentration of added NaCl leads to an increased droplet formation, nevertheless, this needs to be confirmed by several more rounds of observations. Lin et. al, 2015, however, found that droplet formation is favored by low salt conditions, while working with an RNP granule system. These opposing observations might be the result of the different protein system used or the absence of RNA in µNS. Further, we could only detect an increased formation of aggregation over time an no change in number of the droplets, as opposed to findings from Brandariz-Nuñez et al.; 2010. However, those aggregates must have been caused by impurities, as the globular inclusions were still present and unchanged in their shape. This contrasts Lin et. al, 2015, as they could observe a morphological change from well-defined globules to more irregularly shaped particles over time. We therefore concluded, that changes such as fusion of single viroplasms, must already occur at much shorter time scales (e.g. during the purification process) or under different environmental conditions.

When analyzing the size distribution of the µNS-globules, we found the majority of droplets exhibited a diameter between 0.80 and 1.19 µm (Figure 26). The histogram from the 50 mM NaCl buffer (Figure 26 c.), however, does not show any similar behavior and droplet diameters between 0.80 and 3.59 µm were observed. With these findings we can now only conclude the typical viroplasm size, but not definitely give a trend for how this size distribution is affected by a change of the NaCl concentration of the surroundings. It could be said, that higher salt would allow the droplets to become bigger (i.e. fuse together), as results of the 200 mM and 500 mM NaCl condition show a comparably high number of droplets in the 1.20

to 1.59 µm range (Figure 29). Further, at higher salt concentration (200 and 500 mM), as opposed to low salt concentration (0 and 20 mM), droplet diameters of up to 2.39 µm were reached. Nevertheless, with 4 droplets showing a diameter between 1.60-2.39 µm, the number of these larger droplets is still quit low compared to the number reached in smaller diameter ranges (0.40-1.59 µm).

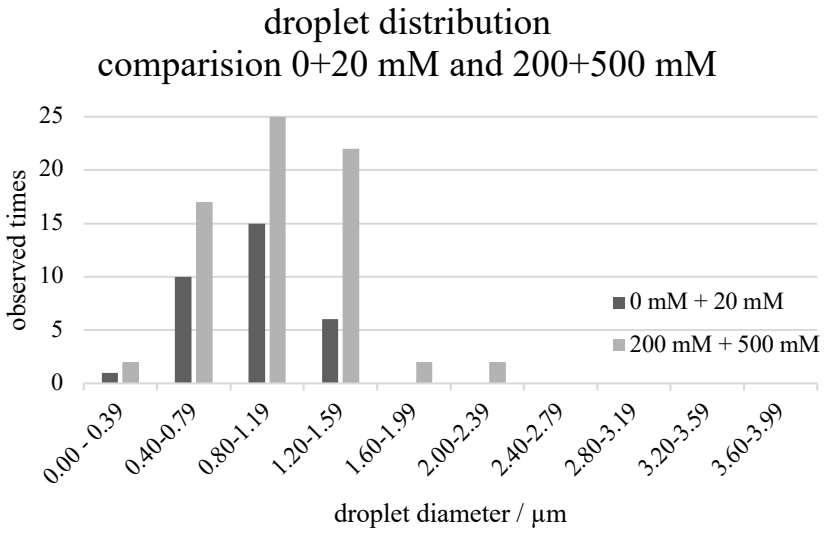

Figure 29 **Droplet size distribution.** Comparison of low salt concentration (0 and 20 mM NaCl) to high NaCl buffer (200 and 500 mM). Droplet diameters in the low salt buffer are in the range of 0.01 to 1.59 µm, those in the higher salt buffer were found to be between 0.01 and 2.39 µm.

Another interesting aspect lies in the presence of the two coiled-coils close to the C-terminus of µNS (Benavente & Martínez-Costas, 2007; Brandariz-Nuñez et al.; 2010). These ordered secondary structures were again visible in the measured CD spectrum (Figures 16 and 17), which indicated the presence of α-helices. By combining these findings with the conducted analysis of the protein sequence (Figure 4), which showed only a few disordered sites, it was concluded, that in the case of µNS, phase separation might be majorly driven by mentioned ordered regions and not only dependent on the presence of disordered regions, which are assumed to be the crucial site in several other proteins (Lin et al., 2015; Nott et al., 2015; Molliex et al., 2015).

Next, we compared the outcome of treating the sample with different concentrations of either NaCl or PEG buffer. In the conditions with additional PEG, the amount of fluorescent globules seemed to be higher, which is supported by previous research, stating that crowding agents (such as PEG) could possibly drive phase separation (Lin et al., 2015). However, in this thesis, the globules were mostly static or attached to the surface as opposed to the often single

and free-floating inclusions detected after treatment with NaCl (Figure 19). Following that, we decided not to proceed with experiments concerning the PEG buffer, as our main focus lay on finding such free-floating droplets.

Several rounds of purification from inclusion bodies and following fluorescent experiments showed, that this specific approach might be unsuitable for proper observation of viroplasms, as the amount of impurities and aggregation was significantly higher (Figures 13 and 25). Nevertheless, we were able to see a small amount of globules (however considerably less than in tests with proteins from the soluble phase (after ultracentrifugation)), so if the purification process can be adapted and optimized, there might be the opportunity to continue with this approach.

Further, thy crystal structure of the µNS protein remains unsolved. Finding suitable conditions for crystal growth could allow X-ray diffraction measurements and subsequent structural analysis. A resolved structure could possibly offer new views on how the protein interacts structurally with either other µNS particles or how it recruits σNS into viroplasms (Touris-Otero et al., 2004). Therefore, a minor part of this thesis focused on finding such optimal growth conditions. We tested several different crystal screens, however, mostly generated salt crystallization or very small protein crystals (Figure 27 and 28). As these cannot be used for further structural analysis, the process still needs to be optimized in future. Another approach could be to adapt the purification protocol to verify whether or not unsuccessful crystallization is a result of not sufficiently pure samples.

Generally, the storage of the expressed and purified µNS-mNeon complex caused several issues throughout this thesis. Over the first months, the samples were stored in the dark at 4°C, which seemed to be suitable concerning the stability of the protein (and fluorophore). However, as we tried to re-observe samples, which exhibited viroplasm formation in the first round of fluorescence experiments, we were only able to detect a fraction of the initial background fluorescence. It was then concluded, that over time, either the fluorophore or the whole complex degrades and loses the ability to emit light after excitation. Following this, it was considered to flash-freeze the samples immediately after purification and store them in the freezer until further use. However, the best results were obtained by observing the sample immediately after its purification.

6. Conclusion

Initially, this thesis was meant to give a clearer view on phase separation in viroplasm formation. For that purpose, it was tried to create a suitable environment for in vitro observations of the µNS protein, as this particular protein has already shown to be the major contributor to such inclusions in the avian reovirus (Tourís- Otero et al.; 2004). On the other hand, proposing a new model for studying phase separation in-vitro would give a new starting point for several other cellular studies. Phase separation itself has not been part of cell biological research for long but has gained interest over the last years as more attention has been put on its physiological relevance in life sciences (Jacobs & Frenkel, 2017; Brangwynne, 2011). Creating a proper environment in which this can be studied could help scientists understand better why, how and under which external conditions these de-mixing events occur.

Testing different types of cell lines showed, that using the *E.coli* competent CODON+ cells (agilent-RIPL) lead to the highest protein yield in both the soluble and insoluble phase. Further, the protein was purified with either metal affinity chromatography (ÄKTA Pure System (GE healthcare)) or a combination of the former and anion-exchange chromatography (ÄKTA Pure system (GE Healthcare)). As mentioned previously, both options generated sufficiently pure samples. However, after HisTag purification, it should be evaluated, based on the purity of the fractions, whether a consecutive round of purification using a HiTrap Q HP column (GE Healthcare) is needed. For purification from inclusion bodies, both the purification procedure as well as the dialysis afterwards, need to be optimized. By now, the number of impurities is still rather high, and the tested dialysis methods lead to a significant lowering of protein concentration.

We could prove, that the µNS protein is indeed forming globular inclusions, as proposed by Touris-Otero et al., 2004. We also confirmed that this can occur in vitro, meaning, that no cellular features such as the microtubule-network are required (Brandariz - Nuñez et al.; 2010). The observed shapes and dynamics are further indicative of inclusions formed by LLPS (Brangwynne, 2011). However, to gain a deeper knowledge about phase separation, a better way to quantify fluorescence observations is needed. Lastly, the crystallization procedures/conditions need to be optimized further to allow X-ray diffraction.

In future, given the problems with controlling the stability of the purified protein it could be tried to obtain a phase diagram by not focusing on viroplasm formation but its dissociation. This could be interesting, as the tested conditions and procedures already lead to

viroplasm formation in the sample and it would be simpler to add dissociation driving factors, such as 1,6-hexandiol, which disrupts weak hydrophobic interactions (Molliex et al., 2015; Patel et. al., 2007), than to establish a completely new purification protocol.

7. References

Attoui, H., de Micco, P., de Lamballerie, X., Billoir, F., & Biagini, P. (2000). Complete sequence determination and genetic analysis of Banna virus and Kadipiro virus: proposal for assignment to a new genus (Seadornavirus) within the family Reoviridae. Journal Of General Virology, 81(6), 1507-1515. https://doi.org/10.1099/0022-1317-81-6-1507

Banerjee, A., & Shatkin, A. (1970). Transcription In Vitro by Reovirus-Associated Ribonucleic Acid-Dependent Polymerase 1. Journal Of Virology, 6(1), 1-11. https://doi.org/10.1128/jvi.6.1.1-11.1970

Barik, A., Katuwawala, A., Hanson, J., Paliwal, K., Zhou, Y., & Kurgan, L. (2020). DEPICTER: Intrinsic Disorder and Disorder Function Prediction Server. Journal Of Molecular Biology, 432(11), 3379-3387. doi: 10.1016/j.jmb.2019.12.030

Barton, E., Forrest, J., Connolly, J., Chappell, J., Liu, Y., & Schnell, F. et al. (2001). Junction Adhesion Molecule Is a Receptor for Reovirus. Cell, 104(3), 441-451. https://doi.org/10.1016/s0092-8674(01)00231-8

Benavente, J., & Martínez-Costas, J. (2007). Avian reovirus: Structure and biology. Virus Research, 123(2), 105-119. https://doi.org/10.1016/j.virusres.2006.09.005

Boeynaems, S., Alberti, S., Fawzi, N., Mittag, T., Polymenidou, M., & Rousseau, F. et al. (2018). Protein Phase Separation: A New Phase in Cell Biology. Trends In Cell Biology, 28(6), 420-435. https://doi.org/10.1016/j.tcb.2018.02.004

Boyarsky, M., & Semenov, A. MULTICOMPONENT SYSTEMS THERMODYNAMICS. A-To-Z Guide To Thermodynamics, Heat And Mass Transfer, And Fluids Engineering. https://doi.org/10.1615/atoz.m.multicomponent_systems_thermodynamics

Brandariz-Nuñez, A., Menaya-Vargas, R., Benavente, J., & Martinez-Costas, J. (2010). Avian Reovirus μNS Protein Forms Homo-Oligomeric Inclusions in a Microtubule-Independent Fashion, Which Involves Specific Regions of Its C-Terminal Domain. Journal Of Virology, 84(9), 4289-4301. https://doi.org/10.1128/jvi.02534-09

Brangwynne, C. (2011). Soft active aggregates: mechanics, dynamics and self-assembly of liquid-like intracellular protein bodies. Soft Matter, 7(7), 3052. https://doi.org/10.1039/c0sm00981d

Broering, T., Parker, J., Joyce, P., Kim, J., & Nibert, M. (2002). Mammalian Reovirus Nonstructural Protein μNS Forms Large Inclusions and Colocalizes with Reovirus Microtubule-Associated Protein μ2 in Transfected Cells. Journal Of Virology, 76(16), 8285-8297. https://doi.org/10.1128/jvi.76.16.8285-8297.2002

Broering, T., Arnold, M., Miller, C., Hurt, J., Joyce, P., & Nibert, M. (2005). Carboxyl-Proximal Regions of Reovirus Nonstructural Protein μNS Necessary and Sufficient for Forming Factory-Like Inclusions. Journal Of Virology, 79(10), 6194-6206. https://doi.org/10.1128/jvi.79.10.6194-6206.2005

Clavel, D., Gotthard, G., von Stetten, D., De Sanctis, D., Pasquier, H., & Lambert, G. et al. (2016). Structural analysis of the bright monomeric yellow-green fluorescent protein mNeonGreen obtained by directed evolution. Acta Crystallographica Section D Structural Biology, 72(12), 1298-1307. https://doi.org/10.1107/s2059798316018623

Drayna, D., & Fields, B. (1982). Activation and characterization of the reovirus transcriptase: genetic analysis. Journal Of Virology, 41(1), 110-118. https://doi.org/10.1128/jvi.41.1.110-118.1982

Duncan, R. (1996). The Low pH-Dependent Entry of Avian Reovirus Is Accompanied by Two Specific Cleavages of the Major Outer Capsid Protein μ2C. Virology, 219(1), 179-189. https://doi.org/10.1006/viro.1996.0235

Gasteiger E., Hoogland C., Gattiker A., Duvaud S., Wilkins M.R., Appel R.D., Bairoch A.; *Protein Identification and Analysis Tools on the ExPASy Server;*

(In) John M. Walker (ed): The Proteomics Protocols Handbook, Humana Press (2005). pp. 571-607

Jacobs, W., & Frenkel, D. (2017). Phase Transitions in Biological Systems with Many Components. Biophysical Journal, 112(4), 683-691. https://doi.org/10.1016/j.bpj.2016.10.043

Labrada, L., Bodelón, G., Viñuela, J., & Benavente, J. (2002). Avian Reoviruses Cause Apoptosis in Cultured Cells: Viral Uncoating, but Not Viral Gene Expression, Is Required for Apoptosis Induction. Journal Of Virology, 76(16), 7932-7941. https://doi.org/10.1128/jvi.76.16.7932-7941.2002

Lin, Y., Protter, D., Rosen, M., & Parker, R. (2015). Formation and Maturation of Phase-Separated Liquid Droplets by RNA-Binding Proteins. Molecular Cell, 60(2), 208-219. https://doi.org/10.1016/j.molcel.2015.08.018

Martínez-Costas, J., Grande, A., Varela, R., García-Martínez, C., & Benavente, J. (1997). Protein architecture of avian reovirus S1133 and identification of the cell attachment protein. Journal Of Virology, 71(1), 59-64. https://doi.org/10.1128/jvi.71.1.59-64.1997

Martinez-Costas, J., Varela, R., & Benavente, J. (1995). Endogenous Enzymatic Activities of the Avian Reovirus S1133: Identification of the Viral Capping Enzyme. Virology, 206(2), 1017-1026. https://doi.org/10.1006/viro.1995.1024

Martinez-Costas, J., Varela, R., & Benavente, J. (1995). Endogenous Enzymatic Activities of the Avian Reovirus S1133: Identification of the Viral Capping Enzyme. Virology, 206(2), 1017-1026. https://doi.org/10.1006/viro.1995.1024

Mertens, P. (2004). The dsRNA viruses. Virus Research, 101(1), 3-13. https://doi.org/10.1016/j.virusres.2003.12.002

Molliex, A., Temirov, J., Lee, J., Coughlin, M., Kanagaraj, A., & Kim, H. et al. (2015). Phase Separation by Low Complexity Domains Promotes Stress Granule Assembly and Drives Pathological Fibrillization. Cell, 163(1), 123-133. doi: 10.1016/j.cell.2015.09.015

Morozov, S. (1989). A possible relationship of reovirus putative RNA polymerase to polymerases of positive-strand RNA viruses. Nucleic Acids Research, 17(13), 5394-5394. https://doi.org/10.1093/nar/17.13.5394

Nibert, M.L., Schiff, L.A., 2001. Reoviruses and their replication. In: Knipe, D.M., Hooley, P.M. (Eds.), Fields Virology, fourth ed. Lippincott Willams & Wilkins, Philadelphia, PA, pp. 1679–1728.

Nott, T., Petsalaki, E., Farber, P., Jervis, D., Fussner, E., & Plochowietz, A. et al. (2015). Phase Transition of a Disordered Nuage Protein Generates Environmentally Responsive Membraneless Organelles. Molecular Cell, 57(5), 936-947. doi: 10.1016/j.molcel.2015.01.013

Patel, S., Belmont, B., Sante, J., & Rexach, M. (2007). Natively Unfolded Nucleoporins Gate Protein Diffusion across the Nuclear Pore Complex. Cell, 129(1), 83-96. doi: 10.1016/j.cell.2007.01.044

Shaner, N., Lambert, G., Chammas, A., Ni, Y., Cranfill, P., & Baird, M. et al. (2013). A bright monomeric green fluorescent protein derived from Branchiostoma lanceolatum. Nature Methods, 10(5), 407-409. https://doi.org/10.1038/nmeth.2413

Spandidos, D., & Graham, A. (1976). Physical and chemical characterization of an avian reovirus. Journal Of Virology, 19(3), 968-976. https://doi.org/10.1128/jvi.19.3.968-976.1976

Touris-Otero, F., Martínez-Costas, J., Vakharia, V., & Benavente, J. (2004). Avian reovirus nonstructural protein μNS forms viroplasm-like inclusions and recruits protein σNS to these structures. Virology, 319(1), 94-106. https://doi.org/10.1016/j.virol.2003.10.034

Zhang, X., Tang, J., Walker, S., O'Hara, D., Nibert, M., Duncan, R., & Baker, T. (2005). Structure of avian orthoreovirus virion by electron cryomicroscopy and image reconstruction. Virology, 343(1), 25-35. https://doi.org/10.1016/j.virol.2005.08.002

8. Appendix

8.1 sequences of the protein μNS and the fluorescent tag mNeon

https://www.ncbi.nlm.nih.gov/nuccore/KC295282.1

>KC295282.1 Synthetic construct monomeric green fluorescent protein (mNeonGreen) gene, complete cds
ATGGTGAGCAAGGGCGAGGAGGATAACATGGCCTCTCTCCCAGCGACACATGAGTTACACATCTTTGGCT
CCATCAACGGTGTGGACTTTGACATGGTGGGTCAGGGCACCGGCAATCCAAATGATGGTTATGAGGAGTT
AAACCTGAAGTCCACCAAGGGTGACCTCCAGTTCTCCCCCTGGATTCTGGTCCCTCATATCGGGTATGGC
TTCCATCAGTACCTGCCCTACCCTGACGGGATGTCGCCTTTCCAGGCCGCCATGGTAGATGGCTCCGGAT
ACCAAGTCCATCGCACAATGCAGTTTGAAGATGGTGCCTCCCTTACTGTTAACTACCGCTACACCTACGA
GGGAAGCCACATCAAAGGAGAGGCCCAGGTGAAGGGGACTGGTTTCCCTGCTGACGGTCCTGTGATGACC
AACTCGCTGACCGCTGCGGACTGGTGCAGGTCGAAGAAGACTTACCCCAACGACAAAACCATCATCAGTA
CCTTTAAGTGGAGTTACACCACTGGAAATGGCAAGCGCTACCGGAGCACTGCGCGGACCACCTACACCTT
TGCCAAGCCAATGGCGGCTAACTATCTGAAGAACCAGCCGATGTACGTGTTCCGTAAGACGGAGCTCAAG
CACTCCAAGACCGAGCTCAACTTCAAGGAGTGGCAAAAGGCCTTTACCGATGTGATGGGCATGGACGAGC
TGTACAAGTAA

https://www.ncbi.nlm.nih.gov/protein/459360587

>AGG56535.1 monomeric green fluorescent protein [synthetic construct]
MVSKGEEDNMASLPATHELHIFGSINGVDFDMVGQGTGNPNDGYEELNLKSTKGDLQFSPWILVPHIGYG
FHQYLPYPDGMSPFQAAMVDGSGYQVHRTMQFEDGASLTVNYRYTYEGSHIKGEAQVKGTGFPADGPVMT
NSLTAADWCRSKKTYPNDKTIISTFKWSYTTGNGKRYRSTARTTYTFAKPMAANYLKNQPMYVFRKTELK
HSKTELNFKEWQKAFTDVMGMDELYK

https://www.ncbi.nlm.nih.gov/nuccore/MK416138.1

>MK416138.1 Avian orthoreovirus strain K1600600 MuNS gene, complete cds
CTAGCGTGGATCATGGCGTCAACCAAGTGGGGAGACAAGCCGATGTCGCTCTCAATGTCTCACGATGGAT
CATCTATCCGCAGTGCCGCCTCACAATTTCTGTCTGTTCCCCTGTCTCACTCAACGCCGATCCCACCTCA
ACGGAAGACCGTACTGCTGAAATTCATGATTGGTGATGACCTGGTTACCGTTCAGGGCGCCCTCGCTCCT
TTTGATGAGTACTGGTACGATAATCAACCGCTATTGTCTCAGGCTGTTGAGCTGCTCGCTTCTGAGGATC
GTCTACGTCAATTTGAGCATTATGAGAAATTTCTGCTTAAGAAGGGCCACCAAATCGCTGAGATCATGAA
CAGGCTACGTCTTTTCTTCACTGACGTTCTCAAAGTGAAGATGGAAGCTGATGCTCTTCCTTCTCTGGCT
CAATACCTAATGGCTGGTACGTTGGATGCCGTCTCCAACGTTCACGAACCTGATGCTTGTGTTCCAGTCA
CTTCAAAGATCATAGCTAAGCAGCAGACCGTGTCCAAGTCCCCTGGACGTCTTGATGAAGAGGAGTATAA
TGTCATTAGATCACGTTTCCTCACTCATGAGATCTTTGACTTAACGTCCGACTTGCCCGGTGTTCAACCA
TTCATGGATATGTACTATGCCACCGTTCCTCGTGCCGATTCCACCGGTTGGTGTGTCTACCGTAGAAAAG
GTCTGTTGATCCATGCCCCTGACGAGCAATACTCGGATCTGACTATCTTCACCACCCGTCTTACGGCAGC
ACGTGAGTTACAGCTCGTGGCTGGGGAGGTCGTTGTGGCTTGTTTCGATCTTATGGATGTCTCTGACATT
GCTCCATCTCATCACGCATCAGTTCAAGAGGAACGTACTCTCGGTACTAGTAGGTACTCCAACGTCACAG
CTAACGAGCATCCGTTGGTATTCTTTTCACCCAATGCACTACGTTGGGCAATAGATCATGCCTGTACTGA
TTCCTTGATTTCCACTAGGAATATCCGGGTATGTGTTGGCATCGATCCCTTAGTGACCAGATGGACTCGC
GATGGCGTGCAGGAGGCTGCTATTCTTATGGATGACAAGCTACCCTCAGCAGGACGTGCTCGTATGGCTC
TACGAACGTTACTTCTAGCGCGTCGATCACCAATGACATCCTTCTTACTAGGTGCTCTCAAGCAGTCCGG
TGGTCAGCTAATGGAACACTATCGATGTGATGCGGCTAACAGGTATGGATCGCCCACCATTCCAGTTTCT
CACCCTCCACCGTGTCCAAAATGTCCTGAGTTGAAGGAACAGATCACCAAACTTTCGTCAGCTCCTGCGC
CTAAGGTTGACTCGTCTGCTGGCCCAGCCGTGCTGTTGTCGAAAATTGCTGAGCTCCAGCGTGCTAACCG
AGAACTGTCTCTGAAGTTAGTGGACGTTCAGCCGGCTCGAGAAGACCACCTTCTAGCTTACCTTGATGAG
CACGTATGCGTTAACGCTAAAGATCATGAGAAAGGTCTACTCGCCCGCTGTAATGTCTCGAGTGATTCAA
TCACCGCTATCCTTGGCCAACGTTTGAAAAATCGAGAACGGTTTGAAACGAGACTACGGCACGAGGCTGR
TGCTGAGTGGGAGCCACGAGTGGAAGCGTTAAATCAAGAGTTGGCTAAGGCGCGTATTGAGCAACAAGAT
ATGATGACTCAGTCCTTACAGTACCTAAACGAGCGTGATGAACTGTTGCACGAGGTGGATGAGCTTAAGC
GTGAACTGACTACCTTACGGTCTGCTAATATGAGACTAAATGCCGATAACCACCGTATGAGCCGTGCGAC
CCGTGTTGGAGATGTATTCGTCAGTGATGTTGATCCCTTACCTCTCAGCCTCCCTGGTGAATCGAAACCG
TCCATTGAAGAACTGGTAGATGATCTGTGAGCTTTGACTTGTGACTCGACTTCTCTCTGATTCCATGTAC
CCACGGCGGACTCG

8.2 basic features of pET 19b

Novagen

pET-19b Vector

TB049 12/98

The pET-19b vector (Cat. No. 69677-3) carries an N-terminal His•Tag® sequence followed by an enterokinase site and three cloning sites. Unique sites are shown on the circle map. Note that the sequence is numbered by the pBR322 convention, so the T7 expression region is reversed on the circular map. The cloning/expression region of the coding strand transcribed by T7 RNA polymerase is shown below.

pET-19b sequence landmarks

T7 promoter	472-488
T7 transcription start	471
His•Tag coding sequence	366-395
Multiple cloning sites	
(*Nde* I - *Bam*H I)	319-335
T7 terminator	213-259
lacI coding sequence	875-1954
pBR322 origin	3891
bla coding sequence	4652-5509

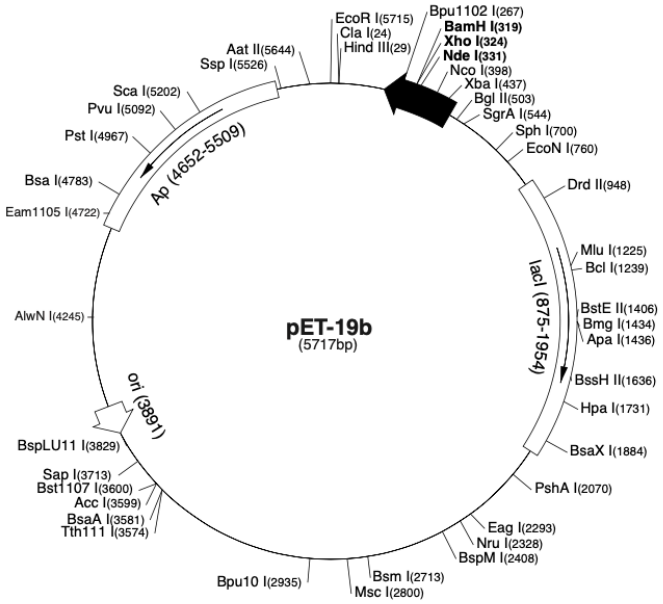

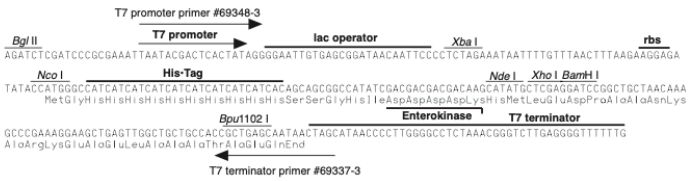

pET-19b cloning/expression region